Deytec Technical Report No. 2009-02

Validation of the CFAST and FDS Fire Models with Large Fire Experiments in a Compartment

Deytec, Inc.

Nuclear Engineering Services

Validation of the CFAST and FDS Fire Models with Large Fire Experiments in a Compartment

March 2009

Prepared by
Dr. Monideep K. Dey

HC-64, Box 100-27
Yellow Spring, WV 26865
USA

Deytec, Inc.
Nuclear Engineering Services

© Deytec, Inc. 2009. All rights reserved.

This document is copyrighted. It is the property of Deytec, Inc. It may be cited but not reproduced, distributed, published, or used by any other individual or organization for any other purpose whatsoever unless written permission is obtained from Deytec, Inc.

Abstract

The analysis presented in this report was conducted for Benchmark Exercise # 4 in the International Collaborative Fire Model Project (ICFMP). The analysis was conducted with the Consolidated Model for Fire and Smoke Transport (CFAST), a zone model, and the Fire Dynamics Simulator (FDS), a computational fluid dynamic model developed by the Building Fire Research Laboratory (BFRL), National Institute of Standards and Technology (NIST). The U.S. Nuclear Regulatory Commission (NRC) is evaluating the CFAST and FDS fire models developed by the National Institute of Standards and Technology for use in NRC's regulatory framework. The objective of the 4th benchmark exercise was to examine scenarios in a compartment with intense fire sources. FDS, including its output processor Smokeview, provides a useful tool to examine the phenomena involved in the scenarios, specifically for examining the flow patterns and behavior through the door or ventilation opening. The trends of the results from FDS show that the code contains the physics and is capable of simulating the complex phenomena in the fire scenarios in this exercise. However, CFAST in its current form is unsuitable for simulating these scenarios. Although relatively good general performance is observed for FDS, the heat flux models (for radiation and convection) and target models in FDS require improvement before they can be reliably used for NPP applications. The code also requires improvement to accurately simulate plume behavior and tilting due to varying flow conditions in a compartment.

Table of Contents

List of Tables

List of Figures

Executive Summary

The analysis presented in this report was conducted for Benchmark Exercise # 4 in the International Collaborative Fire Model Project (ICFMP). The analysis was conducted with CFAST, a zone model, and FDS, a computational fluid dynamic model (CFD) developed by the National Institute of Standards and Technology. The U.S. Nuclear Regulatory Commission (NRC) is evaluating the CFAST and FDS fire models developed by the National Institute of Standards and Technology for use in NRC's regulatory framework. The objective of the 4th benchmark exercise was to examine scenarios in a compartment with intense fire sources. The fire scenarios in Benchmark Exercise #4 are considered to be the most complex and severe that analysts would model for NPP applications. The scenarios apply to either a very large fire size to compartment volume ratio, or applications involving the calculation of heat fluxes and target response near the fire.

FDS, including Smokeview, provides a useful tool to examine the phenomena involved in the scenarios. The tools were useful in deriving interesting observations regarding the flow pattern and behavior through the door or ventilation opening. The FDS code demonstrated the capability to simulate the severe fire scenarios in Benchmark Exercise # 4. Temperatures in these scenarios reached 1000 C, and heat fluxes of upto 100 kW/m2 were observed. These ranges represent the most extreme thermal environments one might expect in NPP applications. The accuracy of the model for computing local gas temperature is best.

Several difficulties were encountered with the CFAST code including instabilities in the computation of several parameters. Although the CFAST prediction of global parameters (HGL temperature, interface height) was within 20 %, CFAST predicted unrealistic values for heat flux to the targets and walls, and the corresponding target and wall temperatures.

There were convergence issues in the CFAST simulation of the more severe test. The simulation halted before completion. CFAST is sensitive in cases with a high heat flux. The penetration of the thermal wave in the compartment floor and in less dense materials with low thermal conductivity poses numerical challenges for the CFAST code causing the simulation to halt before the end of the transient. Although the CFAST model could be used to compute global parameters for the less severe scenario in this benchmark exercise, its use is limited and not recommended for computing heat fluxes and target responses due to the limitations noted above. For more severe scenarios, the two zone approximation and inherent weaknesses in the code limit its applications. The CFAST model is unsuitable for these scenarios with intense fire sources.

Although relatively good general performance is observed for FDS, the error of the heat flux predictions by FDS can be large (upto 59 %). There are specific weaknesses in the heat flux models in FDS which make it unreliable for predicting heat fluxes to targets in NPPs.

The FDS code also requires improvement to accurately simulate plume behavior and tilting due to varying flow conditions in a compartment. FDS computations of the plume predict a larger tilt due to flow conditions, whereas, the plumes in the experiments are observed to be stiffer and influenced less by flow conditions. This inaccuracy in FDS limits the reliability of using FDS to evaluate targets near the plume.

A detailed heat transfer model for the barrel target used in the experiments will be fairly complex. The CFAST and FDS fire models are not capable of modeling complex configurations such as the barrel for storing radioactive waste. The cylindrical geometry and multi-material composition poses challenges for modeling. Similar limitations of CFAST and FDS for modeling cable targets were noted in ICFMP Benchmark Exercise # 1 [Dey, 2002]. The large uncertainties in the prediction of heat flux to the targets limit the reliability of using FDS or CFAST for predicting target temperatures. Lack of ability to model targets other than rectangular slabs, e.g. radioactive waste barrels, limit the usefulness of the codes for NPP target analysis.

Although the fluid dynamics of the scenario is simulated well by FDS, the simple extinction model in FDS (LOL) decreases the heat output from the fire in the more severe scenario when in reality combustion is fully sustained. The algorithm in FDS for accounting for the under ventilation of the fire is too simplistic for complex scenarios as in this benchmark exercise.

The CFAST and FDS codes do not have the capability to model multi-layer boundaries, therefore, a single-layer assumption had to be adopted to model the multi-layer boundaries in this benchmark exercise. Further, the multi-layer composition of the target barrel could not be modeled, although the modeling of the cylindrical geometry is a more fundamental limitation. The use of these codes for complex target geometries and composition is very limited.

The CFAST model requires major fundamental improvements if it is to be used for fire scenarios with intense fire sources such as those examined in this benchmark exercise. The heat flux models (for radiation and convection) and target models in FDS require improvement before they can be reliably used for NPP applications. The simple algorithms for modeling extinction in FDS should be corrected to maintain the HRRs prescribed by the user to improve the performance and accuracy of the model. The basic extinction phenomena requires a more fundamental treatment in FDS to be able to predict under ventilated conditions. Finally, the ability to simulate multi-layer boundaries and targets needs to be implemented in FDS for NPP applications.

The tests used in this benchmark exercise provide fire scenarios with intense fire sources in a compartment. It will be beneficial to conduct tests that provide a range of fire intensities so that one can determine the limits of zone models over which their theoretical formulations remain valid.

Acknowledgments

The author wishes to acknowledge the efforts of GRS and IBMB for developing the specification of this exercise for the International Collaborative Fire Model Project. It is recognized that development of such a specification and experimental data requires considerable resources from these organizations. Specifically, the efforts of Walter Klein-Hessling and Marina Rowekamp at GRS, and R. Dobbernack and Olaf Riese at iBMB are greatly acknowledged and appreciated. Also, the author thanks the many participants of the International Collaborative Project and this benchmark exercise for their comments on the analysis reported herein, and the useful discussions on the complex fire scenarios analyzed in this exercise.

1 Introduction

The validation study of the CFAST and FDS fire computer codes presented here was conducted as part of Benchmark Exercise # 4 of the International Collaborative Fire Model Project (ICFMP). The USNRC exercised the CFAST and FDS codes, developed by the National Institute of Standards and Technology (NIST), as part of its program to evaluate and validate these computer codes for use in NRC's regulatory framework. A complete specification of the exercise is included in Appendix A. The following provides a summary of the specification of the benchmark exercise.

1.1 Specification of International Benchmarking Exercise # 3

Experiments with large pool fires in a compartment conducted at iBMB (Institut für Baustoffe, Massivbau und Brandschutz) of Braunschweig University of Technology, Germany were used for this benchmark exercise.

1.1.1 Room Geometry

The experimental room (see Figure 1.1) has a floor area of 3.6 m x 3.6 m and a height of 5.7 m. The room is made of concrete and is naturally and mechanically ventilated. The surface materials as well and the thermophysical properties of those materials are listed in Tables 1-1

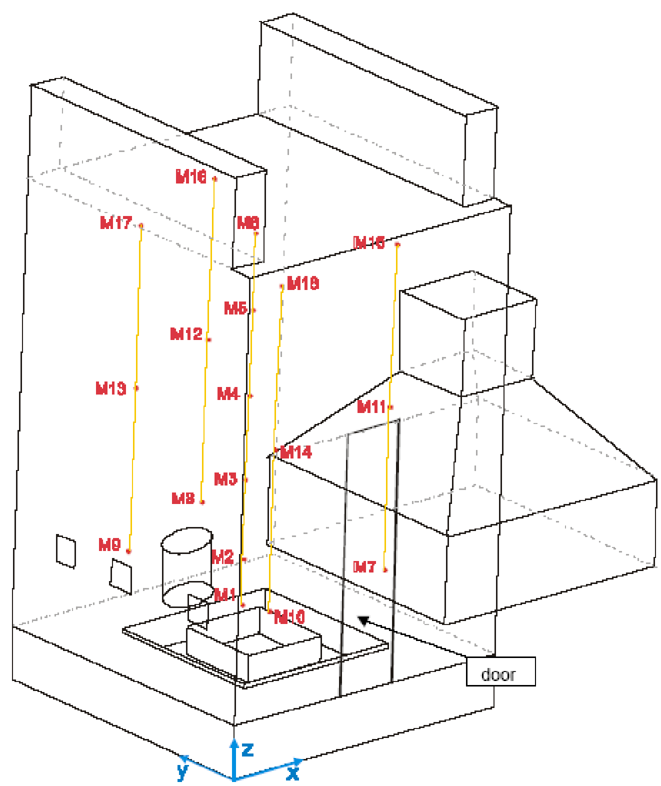

Figure 1.1 Compartment for Benchmark Exercise # 4

and 1-2.

Table 1-1 Wall, Floor, and Ceiling Material

Surface	Material	Thickness [m]
Floor	Concrete	0.3
	Aereted concrete	0.6
Side walls	Light concrete	0.25
	Insulation	0.05
Ceiling	Concrete	0.25
	Insulation	0.05
Side walls channel	Light concrete	0.125
	Insulation	0.06
Ceiling channel	Concrete	0.13
	Insulation	0.07

Table 1-2 Thermophysical Properties of Wall, Floor, and Ceiling Materials

Material	Thermal conductivity [W/m K]	Specific Heat [kJ/kg K]	Density [kJ/m^3]
Concrete	2.10	880	2400
Aerated concrete	0.75	840	1500
Light concrete	0.11	1350	420
Insulation	0.05	1500	100

1.1.2 Natural Ventilation

In Test 1, an open door (see Fig. 1.1) is located at the center of front wall (x = 1.8; y = 0). The door has an area of 0.7 m x 3.0 m. The lower edge of the door is just above the aerated concrete (see section 1.1.4 for further details) at z = 0.6 m. All other doors are closed.

In Test 3, the door opening was partly closed. The free cross section was reduced to 0.7 m x 1.0 m and opening starts at an elevation of 1.6 m (1 m above the aerated concrete bottom surface).

1.1.3 Mechanical Ventilation

There are two ventilation ducts with the width of 0.42 m and a height of 1.03 m at the ceiling. The length of both ducts is approximately 3.625 m and leads to the fan system. Although the fan system was not in use, flow velocities were measured.

1.1.4 Fire

In the center of the floor area, a pan with a size of 4 m^2 has been installed on a weight scale. The bottom level of this pan has an elevation of about 0.36 m. The depth is approximately 0.3 m high. The kerosene mass loss is measured with the scale. To protect this measurement aerated concrete has been applied around this pan on the complete floor area up to an elevation of 0.6 m. Also, the inner side of the large pan was covered by 0.05 m thick light concrete plates for protection.

In the center of the large pan, a smaller1 m^2 pan has been installed. The bottom of this pan has an elevation of about 0.51 m. The depth is 0.2 m. For stabilization a 0.03 m wide steel plate has been installed around the upper edge of the pan side-wall.

A hood was installed above the front door (See Figure 1-1). Using the oxygen consumption method the energy release can be estimated.

1.1.5 Targets

Three different types of material probes have been positioned on the right side of the fire compartment (x = ~ 0 m). The materials are "aerated concrete ", concrete and steel. The size of these elements is 0.3 m x 0.3 m. The thickness is 0.1 m for the concrete probes and 0.02 m for the steel plate. The properties of the materials are listed in Table 1-2. The location of the center surface is also given in Table 1-3. The sensor M29 represents the aerated concrete material. Sensors M33 and M34 represents the concrete and steel materials, respectively.

Table 1-3 Target Description and Location

			Fire Location [m]			
			X	**Y**	**Z**	
			1.8	1.8	0.51	
			Target Location [m]			Distance to
ID	**Description**	**Orientation**	**X**	**Y**	**Z**	Fire [m]
M29	Gas concrete material	Pointing at fire	0.08	0.65	1.7	2.39
M33	Concrete material	Pointing at fire	0.08	1.9	1.7	2.09
M34	Steel material	Pointing at fire	0.02	2.8	1.7	2.36

2 Input Parameters and Assumptions

A comprehensive specification of Benchmark Exercise # 4 was developed such that there would be a minimal amount of unspecified parameters and assumptions for the analysts conducting predictions for the Specified Calculations per ASTM 1355-05 [ASTM, 2005]. However, there were still some parameters for which values had to assumed for conducting the Specified Calculations. These are listed and discussed below:

1. Fire Growth: An evaluation of the FDS code to simulate fire growth and burning rate of the kerosene in the fuel pan was not attempted in this validation study. Although the capability to simulate burning rate exists in theory in the FDS code, it is acknowledged that such sub-models have inherent limitations that cannot be overcome until further research in this area. This research is summarized later in Section 4.4. Also, the simulation of fire growth will require a solid to liquid heat transfer model in FDS to predict the heat up of the fuel pan. Therefore, the heat release rates (HRRs) measured during the experiments were used for this validation study. The use of prescribed heat release rates neglects the feedback effect between the fire and the compartment conditions. Therefore, the use of prescribed HRRs will include some uncertainty due to the lack of complete simulation of the fire phenomena in the compartment.

2. Heat Release Rate (HRR): As indicated above, the HRRs of the fire measured during the experiments were used for this validation study. However, the heat release rate measured during the end of the transient when the fuel level in the pan was low has a large uncertainty associated with it. Oscillations in the heat release rate are noted and may be due to the method used to deduce heat release rates from the derivative of mass loss rate. The value of this parameter, especially during the oscillations and at the peak of the transient, is likely to be the largest source of uncertainty in the predicted results.

3. Lower Oxygen Limit (LOL): The lower oxygen limit needs to be input to the CFAST code for the simplistic sub-model for predicting the extinction of the fire. There was no value for LOL included in the specifications, allowing judgment from users to define the most appropriate value for the experiments. The specification of this parameter has a large effect on the prediction of extinction and could be a large source of user effects[1]. The FDS code has a similar scheme to extinguish the fire when oxygen levels decrease below a preset value and temperatures remain sufficiently high, however, the user does not need to specify the values. The uncertainty in specifying the LOL may have an impact on the predicted results if the fire growth is under-ventilated during the transients.

4. Target Specification: A detailed heat transfer model for the barrel used in the experiments will be fairly complex. The CFAST and FDS fire models are not capable of modeling complex configurations such as the barrel for storing radioactive waste. The

[1]Test 1 was not under ventilated so the LOL did not impact the simulation. CFAST did not successfully simulate Test 3, as discussed later in Chapter 3. The LOL value chosen would have had an impact on this simulation, if it was successfully completed.

cylindrical geometry and multi-material composition poses challenges for modeling. No attempt was made at developing a set of assumptions for the target in the CFAST and FDS codes such that predictions of the temperatures in the barrel could me made. Similar limitations of CFAST and FDS for modeling cable targets were noted in ICFMP Benchmark Exercise # 1 [Dey, 2002].

5. Material Properties of Walls and Targets: The material properties of the walls, ceiling, floor, and targets were specified for the exercise using values available in the literature for these materials. The properties of the specific materials used in the experiments may vary from the generic values reported in the literature. This may a source of uncertainty in the predicted results.

6. Radiative Fraction: The radiative fraction of the fuel was not specified. The value (0.35) of the radiative fraction available in the literature [SFPE, 1995] for n-dodecane was assumed for the analysis. This assumption may have an impact on the predicted results since this parameter determines the convective and radiative heat flow from the plume in both CFAST and FDS fire codes. This parameter was identified as a key parameter effecting fire compartment conditions in ICFMP Benchmark Exercise # 2 [Miles, 2004].

7. Ventilation Flow : The FUCHS system was simply modeled in CFAST and FDS with prescribed flowrates, without accounting for any feedback effects between the ventilation system and the compartment. Further, the flow through the FUCHS system was assumed to be constant for the CFAST calculations as there is no direct means for providing input for varying ventilation flowrates in the code. The average flowrate was used as input for CFAST. These assumptions will lead to some uncertainty in the predicted results.

8. Grid Size: A grid size of 10 cm was used for the FDS calculations. It is recognized that CFD calculations are generally sensitive to the grid used. A grid size of 10 cm may be optimal for the type of scenarios simulated, however, this was not confirmed through a grid sensitivity analysis.

9. Multi-Layer Boundaries: The CFAST and FDS codes do not have the capability to model multi-layer boundaries, therefore, a single-layer assumption had to be adopted to model the aerated concrete around the fuel pan and the concrete floor below. It was assumed that the total floor mass consisted of light concrete, with properties in between aerated concrete and concrete, with an equivalent thickness. The layer of insulation covering the walls and ceiling was neglected in the calculations since it could not be directly modeled in CFAST or FDS.

10. Exhaust Hood: FDS calculations were conducted with and without the exhaust hood above the door of the compartment to determine its effect on the compartment conditions. It was determined that modeling the hood had very little effect on the compartment conditions. Therefore, no attempt was made to account for the exhaust hood as part of a ventilation system in the CFAST calculations.

11. Heat Flux Comparisons: The comparison of heat flux prediction with measured data poses several challenges. It is important that equivalent measures of heat flux are used

in the comparison. The flux gauges in the experiments in benchmark Exercise # 4 were cooled and maintained at a constant temperature (10 C). The CFAST and FDS codes normally output the net heat flux on targets based on the target temperature. It is important that these fluxes be modified to the incident radiative heat flux and the convective heat flux to a block at constant temperature for comparison with measured heat fluxes. Even with the modifications to account for the differences between measured and predicted values, an exact comparison is not possible due to the lack of ability to exactly measure the calculated values from models. Therefore, the comparison of heat fluxes will have some additional uncertainty due to this limitation.

3 Evaluation of Specified Model Predictions

The following provides a comparison of Specified Calculations per ASTM 1355-05 with CFAST and FDS for the tests conducted for ICFMP Benchmark Exercise #4. The results of CFAST, a zone model, and FDS, a CFD code, are presented together to allow a comparison and discussion of the capabilities and limitations of the two types of models. The predictions using CFAST and FDS presented below were made and sent to GRS before the experimental data was released by them. GRS has certified the authenticity of the Specified Calculations. The calculations therefore comply with the requirements for Specified Calculations in ASTM-1 355.

The following is a list of the major sub-models implemented in the two fire computer codes for modeling the physical phenomena in the scenarios:

- combustion chemistry (tracking concentrations of oxygen and combustion products)
- plume and ceiling jet flow
- mass and energy balance
- ventilation through doors
- forced ventilation
- heat transfer to boundaries
- heat transfer to targets
- thermal response of the target

The FDS code computes the flows from first principles based on fluid dynamic equations, whereas CFAST utilizes correlations developed from experimental data. The performance of these sub-models is discussed below based on comparison of predicted results with experimental measurements. The theoretical formulation of the two models may be found in Jones, 2004 for CFAST, and McGrattan, 2004 for FDS. The theoretical formulation of these codes are presented in these reports according to the format and content required by ASTM - 1355, “Evaluating the Predictive Capability of Deterministic Fire Models,” [ASTM, 2004]. These reports were sponsored by the U.S. Nuclear Regulatory Commission for referencing in its validation studies as that reported herein.

The FDS code simulated Tests 1 and 3 successfully. The CFAST code simulated Test 1 to the end of the specified transient, however, instabilities were noted as discussed below. There were convergence issues in the CFAST simulation of Test 3. The simulation halted at about 14 % to completion. CFAST is sensitive in cases with a high heat flux. The penetration of the thermal wave in the compartment floor and in less dense materials with low thermal conductivity poses numerical challenges for the CFAST code.

The following presents the comparison of predictions by the CFAST and FDS code with experimental data for Test 1 and Test 3 of the series. The discussion is grouped in categories presented below to evaluate the predictive capability of the models according to the general features and sub-models of the codes:

- Global parameters
- Local gas temperature
- Heat fluxto targets

- Target temperature
- Heat flux to walls
- Wall temperature

3.1 Test 1

Figures 1 to 19 show the comparison of the trends of the predictions of CFAST and FDS with experimental data, and Table 1 shows the peak values predicted by the models and that measured and the uncertainty of the predictions. The uncertainty value tabulated is:
(model prediction at peak- measured value at peak)/(measured value at peak - initial measured value)

A + sign in the uncertainty value means that the model prediction was greater than the measured value, and a - sign means that the model prediction was less than measured value

3.1.1 Global Compartment Parameters

The HRR measured during the test and prescribed as input to the CFAST and FDS models are shown in Figure 1. The HRR increases rapidly to 2500 kW in ~ 253 s, and then increases more gradually to 3500 kW before being extinguished at ~ 1368 s due to fuel depletion.

Figure 2 shows the development of the hot gas layer. Both CFAST and FDS predict the hot gas layer to develop and reach ~ 1 m above the floor in ~ 200 s. The initial development of the HGL shown in Figure 2 based on measured data seems erratic and may be due to discrepancies in the offset in the initiation of the transient . The measured data shows the HGL interface reaches ~ 1.5 m at ~ 600 s. Table 1 shows the steady state HGL interface height predicted by the codes and measured, and the uncertainties in the CFAST and FDS predictions. Both CFAST and FDS under-predict the steady state HGL interface height by - 19 %.

Figure 3 shows the hot gas layer (HGL) temperature. Both CFAST and FDS predictions follow the same rate of temperature increase as the experimental data with CFAST over predicting the increase by a larger amount. It should be noted that the discrepancy in the time at which the temperature begins to increase should be ignored since that is caused mainly by the offset between the predictions and measured data. Once reaching the end of the rapid increase at ~ 360 s, the increase in temperature is greater in the experiment than that predicted by both CFAST and FDS. This discrepancy may be due to smaller heat loss in the experiments due to the presence of insulation that was ignored in the code calculations. Table 1 shows the peak values predicted by the models and that measured. The uncertainty in the predictions for CFAST and FDS are + 20 % and - 17 %, respectively.

Figure 4 shows the O_2 depletion predicted by CFAST and FDS. The O_2 level at GA1-O2, located at 3.8 m above the floor in the HGL (top of door is at 3.0 m), predicted by CFAST and FDS at the end of the transient is 8.9 % and 5.7 %, respectively. The measured O_2 level at the end of the transient is 13.5 %. Since the measured O_2 level does not decrease much after ~ 465 s, there is potentially an error in the measured O_2 level. Therefore, uncertainties of the predictions are not presented here.

3.1.2 Local Gas Temperature

The local gas temperatures in the plume, ceiling jet, and compartment are only predicted by FDS. FDS outputs are shown in Figures 5 and 6. Figure 5 shows an isosurface of the mixture fraction (at a value of 0.062) at 238 s which represents the flame sheet created by FDS at that point. Figure 5 shows that FDS simulates the flame sheet to be significantly pushed toward the rear wall by the flow of ambient air into the compartment through the door. Figure 6 shows a slice profile (at x = 1.8 m) of the gas temperature in the compartment. Figure 6 again shows that FDS simulates that the plume is pushed significantly toward the rear wall.

Figure 7 shows the comparison of measured plume temperatures at M2, M4, and M6 with that predicted by FDS. As shown in Figure 7, FDS predicts peaks in the plume temperature at ~ 50 s. These peaks are explained by the plume development predicted by FDS. Observations of the plume predicted by FDS through Smokeview (the graphical interface for FDS) indicates a steady vertical plume until ~ 50 s when the plume is pushed to the rear wall by flow into the compartment through the door. This causes peaks in the thermocouples, M2, M4, and M6 which are located directly above the fuel pan. The experimental measurements do not indicate this extensive movement of the fire plume. Figure 3-1 in the main text shows a photograph of the fire and plume at steady state conditions in Test 1. The figure shows some degree of plume tilt in the experiment, but not to the extent predicted by FDS. The measured data shows the plume to be fully developed at ~ 105 s after which the plume temperatures increase to ~ 1000 C without any intermediate peaks. The experimental data shows oscillations in the plume temperature, especially near the fire at M2, indicating oscillation of the fire plume to and from the rear wall. FDS predicts the peaks of the plume temperatures to be ~ 800 C. As shown in Table 1, the uncertainty in the predicted values are - 27 %, - 16 %, and - 25 % for M2, M4, and M6, respectively.

Figure 8 shows the local gas temperatures in the compartment at Level 1 for M7, M8, M9, and M10. The measured temperatures show a rapid increase in temperature followed by a more gradual increase until the end of the transient. The temperature measured at M10 is much higher than that measured at M7, M8, and M9. This is due to the tilting of the fire plume toward M10. FDS also shows a rapid increase in temperature followed by large oscillations and unexpected trends. These oscillations may be caused by oscillations in the flow through the door predicted by FDS. The temperature predicted at M8 by FDS is highest since the code predicts the fire plume to be pushed more toward the rear wall, as discussed above. The experimental data shows some oscillations in the temperature at M10 indicating the movement of the plume in and out of that region. Although the peak values predicted by FDS are similar to that measured for M7, M8, and M9, there is an uncertainty of - 43 % for M10 due to the discrepancy in the degree of plume tilt predicted.

Figure 9 shows the local gas temperature in the compartment at Level 2 for M11, M12, M13, and M14. The peak values predicted by FDS are similar to that measured with an error of - 13 % at M14. The effect of plume tilt is not evident at this level since the plume is maintained (see Figure 3-1 in the main text) mainly in the lower level.

Figure 10 shows the local gas temperature in the compartment at Level 3 for M15, M16, M17, and M18. The peak values predicted by FDS are similar to that measured with an error of - 5 % at M18. Again, the effect of plume tilt is not evident at this level since the plume is maintained in the lower level.

3.1.3 Heat Flux to Plate and Block Targets

The comparison of heat flux prediction with measured data poses several challenges. It is important that equivalent measures of flux are used in the comparison. The flux gauges in the experiments were cooled and maintained at a constant temperature (10 C). The CFAST and FDS codes normally output the net heat flux on targets based on the target temperature. These fluxes were modified to the incident radiative heat flux and the convective heat flux to a block at a constant temperature of 10 C. Even with the modifications to account for the differences between measured and predicted values, an exact comparison is not possible due to the lack of ability to exactly measure the calculated values from models.

Figure 11 shows a comparison of the total heat flux predicted by CFAST and FDS with measurements at WS4 on the aerated concrete block. As noted earlier, instabilities are noted in the flux predicted by CFAST. The CFAST code is sensitive in cases with high heat flux. The penetration of the thermal wave in less dense materials poses numerical challenges for the CFAST code. Therefore, uncertainties associated with the aerated concrete block are not reported. The uncertainty of FDS for total heat flux at WS4 at ~ 40 kW/m2 is + 48 %.

Figure 12 shows a comparison of the total heat flux predicted by CFAST and FDS with measurements at WS3 on the concrete block. CFAST significantly over-predicts the heat flux with an uncertainty of + 146 %. The FDS prediction is similar to that measured with an uncertainty of + 14 %.

Figure 13 shows a comparison of the total heat flux predicted by CFAST and FDS with measurements at WS2 on the steel plate. CFAST again significantly over-predicts the heat flux with an uncertainty of + 215 %. The uncertainty in the FDS prediction is + 59 %.

It should be noted that FDS predicts an increase in the heat flux toward the end of the transient, possibly due to the heat flux from the boundaries to the targets. This increase in heat flux toward the end of the transient is not noted in the measurements.

3.1.4 Plate and Block Temperature

Figure 14 shows a comparison of the surface temperature of the aerated concrete block predicted by CFAST and FDS with measurement. Oscillations in the CFAST prediction is observed due to oscillations in the heat flux calculation (see Figure 11) as discussed above. The uncertainty in the FDS prediction is + 19 %.

Figure 15 shows a comparison of the surface temperature of the concrete block predicted by CFAST and FDS with measurement. CFAST significantly over-predicts the temperature with an uncertainty of + 128 %. The FDS prediction is similar to that measured with an uncertainty in the peak value of + 28 %.

Figure 16 shows a comparison of the front surface temperature of the steel plate predicted by CFAST and FDS with measurement. CFAST significantly over-predicts the temperature with an uncertainty of + 111 %. The FDS prediction is similar to that measured with an uncertainty of + 7 %.

Figure 17 shows a comparison of the back surface temperature of the steel plate predicted by FDS with experiment. The FDS prediction is similar to that measured with an uncertainty of + 7 %.

3.1.5 Heat Flux to Walls

Figure 18 shows a comparison of the heat flux on the wall predicted by FDS with experiment. FDS under predicts the heat flux by - 45 %. The experimental values of the heat flux at WS1 and WS3 which are in comparable locations are similar. Although the FDS prediction for heat flux at WS3 was similar to experiment, it under predicts the flux at WS1.

3.1.6 Wall Temperature

Figure 19 shows a comparison of the wall surface temperatures predicted by FDS with experiment. FDS predictions are similar to experimental observations with an uncertainty of - 26 % at M20.

3.1.7 Conclusion

Several difficulties were encountered with the CFAST code, including instabilities in the computation of several parameters. Although the CFAST prediction of global parameters (HGL temperature, interface height) was within 20 %, CFAST predicted unrealistic values for heat flux to the targets and walls, and the corresponding target and wall temperatures.

FDS predictions were similar to experimental observations for most parameters. Global parameters such as the HGL temperature and interface height were within 20 % of experimental values. The local gas temperatures in the compartment and in the plume predicted by FDS were generally within 15 % and 25 % of experimental observations, respectively. The heat flux to the targets and blocks and corresponding temperatures predicted by FDS deviated by 59 % and 28 % from experimental observation, respectively.

3.2 Test 3

As discussed above, there were convergence issues in the CFAST simulation of Test 3. The simulation halted at about 14 % to completion. CFAST is sensitive in cases with a high heat flux. The penetration of the thermal wave in the compartment floor and in less dense materials poses numerical challenges for the CFAST code causing the simulation to halt before the end of the transient. Therefore, only the predictions of FDS are presented here.
Figures 20 to 40 show the comparison of the trends of the predictions of CFAST and FDS with experimental data, and Table 2 shows the peak values predicted by the models and that measured and the uncertainty of the predictions.

3.2.1 Global Compartment Parameters

The HRR measured during the test and prescribed as input to the FDS model is shown in Figure 20. The measured HRR increases rapidly to 1500 kW in ~ 50 s, and then increases more gradually reaching 2700 kW at 850 s. The HRR increases rapidly from this point to 6000 kW at ~ 1050 s before being extinguished. Although the measured HRR was input to the FDS code, the FDS internal calculation of the HRR decreased after the initial rise at ~ 50 s. Although the HRR calculated by FDS started to increase at ~ 200 s, it was less than the measured HRR upto the peak in HRR. This may due to the internal algorithm in FDS that inadvertently decreases the HRR for under-ventilated conditions.

Figure 21 shows the development of the hot gas layer. FDS predict the hot gas layer to develop and reach ~ 0.6 m above the floor in ~ 90 s. The measured data shows the HGL interface starts to level to ~ 1.6 m (bottom of vent) at ~ 95 s. FDS predicts a steady state level is reached more quickly after the initial drop in level compared to experiment. Table 2 shows the steady state HGL interface height predicted by FDS and measured, and the uncertainty in the FDS prediction. FDS under-predicts the steady state HGL interface height by - 24 %.

Figure 22 shows the hot gas layer (HGL) temperature. FDS under predicts the HGL temperature because of the discrepancy in the HRR (discussed above). Table 2 shows the peak values predicted by the model and that measured. The uncertainty of the prediction for FDS is - 32 %.

Figure 23 compares the O2 depletion predicted by FDS with experiment. The FDS prediction is similar to experimental observation until 840 s at which point FDS predicts a rapid reduction in O2 level to 0 %, while experimental observation indicates the O2 level reaches 0 % more gradually at ~ 1095 s. FDS prediction is less than the measured value by ~ 25 % for most of the transient.

3.2.2 Local Gas Temperature

Figure 24 shows an isosurface of the mixture fraction (at a value of 0.062), which represents the flame sheet created by FDS, at 45 s. The flame is simulated as being vertical up to this time. Figure 25 shows an isosurface of the mixture fraction (at a value of 0.062) created by FDS at 130 s. Figure 25 shows that FDS simulates the flame sheet to be significantly pushed toward the rear wall by the flow of ambient air into the compartment through the door at this time. Figure 26 shows a slice profile (at x = 1.8 m, t = 101.5 s) of the gas temperature in the compartment. Figure 27 shows a slice profile (at x = 1.8 m, t = 102 s) of the gas temperature in the compartment. Figure 26 again shows that FDS simulates that the plume is pushed significantly toward the rear wall. However, observations of this temperature slice file in Smokeview shows that FDS simulates the flow through the door to pulsate with a period of ~ 2 s. Figure 26 shows the flow through the door to be bidirectional, whereas Figure 27 shows the end of the cycle of the pulsation when the flow is unidirectional through the door flowing out of the compartment. This pulsating behavior was noted during the experiments and mentioned in Chapter 3 of the main report. The pulsating flow through the door provides sufficient oxygen to the fire and prevents it from being under ventilated.

Figure 28 shows the comparison of measured plume temperatures at M2, M4, and M6 with that predicted by FDS. As shown in Figure 28, FDS predicts peaks in the plume temperature at ~ 50 s in Test 3 as in Test 1. These peaks are explained by plume development predicted by FDS. Observations of the plume predicted by FDS through Smokeview (the graphical interface for FDS) indicates a steady vertical plume develop until ~ 50 s (also see Figure 24) when the plume is pushed to the rear wall by flow into the compartment through the door. This causes peaks in the thermocouples, M2, M4, and M6 which are located directly above the fuel pan. The experimental measurements do not indicate this extensive movement of the fire plume. The measured data shows the plume to be fully developed at ~ 180 s after which the plume temperatures increase to ~ 1000 C without any intermediate peaks. The experimental data shows oscillations in the fire, especially near the fire at M2. FDS predicts the peaks of the plume temperatures to be ~ 800 C. As shown in Table 2, the uncertainty in the predicted values are - 26 %, - 17 %, and - 27 % for M2, M4, and M6, respectively.

Figure 29 shows the local gas temperatures in the compartment at Level 1 for M7, M8, M9, and M10. The measured temperatures show a rapid increase in temperature followed by a more gradual increase until the end of the transient. The temperature measured at M10 and M8 is higher than that measured at M7 and M9. This is due to the tilting of the fire plume toward the back wall. The plume temperature at M10 is higher than at M8 indicating that the tilt is more toward M10, but not as far as M8. FDS also shows a rapid increase in temperature followed by oscillations and a gradual increase in plume temperature. These oscillations are caused by oscillations in the flow through the door predicted by FDS, as discussed above. The experimental data shows some oscillations in the temperature at M10 indicating the movement of the plume in and out of that region. There are notable peaks in the measured data for M7 and M9 at ~ 1230 s due to the more rapid increase in HRR starting at ~ 800 s and peaking at ~ 1100 s. The uncertainty in the local gas temperatures predicted by FDS at M10 is - 33 %.

Figure 30 shows the local gas temperature in the compartment at Level 2 for M11, M12, M13, and M14. There are notable peaks in the measured data for M11 and M13 at ~ 1305 s due to the more rapid increase in HRR starting at ~ 800 s and peaking at ~ 1100 s. The peak values predicted by FDS are similar to that measured with an error of - 24 % at M14.

Figure 31 shows the local gas temperature in the compartment at Level 3 for M15, M16, M17, and M18. There are notable peaks in the measured data for M15, M16, M17, and M18 at ~ 1305 s due to the more rapid increase in HRR starting at ~ 800 s and peaking at ~ 1100 s. The peak values predicted by FDS are similar to that measured with an error of - 27 % at M18.

3.2.3 Heat Flux to Plate and Block Targets

The comparison of heat flux prediction with measured data poses several challenges. It is important that equivalent measures of flux are used in the comparison. The flux gauges in the experiments were cooled and maintained at a constant temperature (10 C). The CFAST and FDS codes normally outputs the net heat flux on targets based on the target temperature. These fluxes were modified to the incident radiative heat flux and the convective heat flux to a block at a constant temperature of 10 C. Even with the modifications to account for the differences between measured and predicted values, an exact comparison is not possible due to the lack of ability to exactly measure the calculated values from models.

Figure 32 shows a comparison of the total heat flux predicted by FDS with measurement at WS4 on the aerated concrete block. There is a large increase in heat flux at ~ 1155 s when the HRR reaches its peak at 6000 kW. The uncertainty of the FDS prediction at WS4 at ~ 71 kW/m2 is - 53 %.

Figure 33 shows a comparison of the total heat flux predicted by FDS with measurement at WS3 on the concrete block. The uncertainty in the FDS prediction at 66 kW/m2 is - 40 %.

Figure 34 shows a comparison of the total heat flux predicted by FDS with measurement at WS2 on the steel plate. The uncertainty in the FDS prediction at 46 kW/m2 is - 23 %.

3.2.4 Plate and Block Temperature

Figure 35 shows a comparison of the surface temperature of the aerated concrete block predicted by FDS with measurement. The uncertainty in the FDS prediction is + 2 %.

Figure 36 shows a comparison of the surface temperature of the concrete block predicted by FDS with measurement. The uncertainty in the FDS prediction is - 33 %.

Figure 37 shows a comparison of the front surface temperature of the steel plate predicted by FDS with measurement. The uncertainty in the FDS prediction is - 33 %.

Figure 38 shows a comparison of the back surface temperature of the steel plate predicted by FDS with experiment. The uncertainty in the FDS prediction is - 34 %.

3.2.5 Heat Flux to Walls

Figure 39 shows a comparison of the heat flux on the wall predicted by FDS with experiment. FDS under predicts the heat flux by - 8 %.

3.2.6 Wall Temperature

Figure 40 shows a comparison of the wall surface temperatures predicted by FDS with experiment. FDS predictions are similar to experimental observations with an uncertainty of - 34 % at M20.

3.2.7 Conclusion

There were convergence issues in the CFAST simulation of Test 3. The simulation halted at about 14 % to completion. CFAST is sensitive in cases with a high heat flux. The penetration of the thermal wave in the compartment floor and in less dense materials poses numerical challenges for the CFAST code causing the simulation to halt before the end of the transient.

FDS predictions were similar to experimental observations for most parameters. Global parameters such as the HGL temperature, interface height, and O2 concentration were within 32 % of experimental values. The local gas temperatures in the compartment and in the plume predicted by FDS were within 33 % and 27 % of experimental observations, respectively. The heat flux to the targets and blocks and corresponding temperatures predicted by FDS deviated by 53 % and 33 % from experimental observation, respectively. The HRR used by FDS was less than input for the simulation due to algorithms in FDS to account for under ventilated conditions. If these algorithms are corrected to maintain the prescribed HRR, the FDS predictions should be even closer to experimental measurements.

4 General Recommendations and Conclusions

The following provides the findings and conclusions of this validation study. The fire scenarios in Benchmark Exercise # 4 are considered to be the most complex and severe that analysts would model for NPP applications. The scenarios apply to either a very large fire size to compartment volume ratio, or applications involving the calculation of heat fluxes and target response near the fire.

4.1 Capabilities

<u>FDS</u>

The FDS code demonstrated capability to simulate severe fire scenarios such as in Benchmark Exercise # 4. Temperatures in these scenarios reached 1000 C, and heat fluxes of upto 100 kW/m2 were observed. These ranges represent the most extreme thermal environments one might expect in NPP applications. The accuracy of the model for computing local gas temperature is best. Most phenomena are predicted reasonable well for the scenarios in the Benchmark Exercise.

4.2 Limitations

4.2.1 General Modeling of Scenario with CFAST

For Test 1, several difficulties were encountered with the CFAST code including instabilities in the computation of several parameters. Although the CFAST prediction of global parameters (HGL temperature, interface height) was within 20 %, CFAST predicted unrealistic values for heat flux to the targets and walls, and the corresponding target and wall temperatures.

Figure 11 shows a comparison of the total heat flux predicted by CFAST with measurements at WS4 on the aerated concrete block. Instabilities are noted in the flux predicted by CFAST. The CFAST code is sensitive in cases with high heat flux. Figure 12 shows a comparison of the total heat flux predicted by CFAST with measurements at WS3 on the concrete block. CFAST significantly over-predicts the heat flux with an uncertainty of + 146 %. Figure 13 shows a comparison of the total heat flux predicted by CFAST with measurements at WS2 on the steel plate. CFAST again significantly over-predicts the heat flux with an uncertainty of + 215 %.

Figure 14 shows a comparison of the surface temperature of the aerated concrete block predicted by CFAST with measurement. Oscillations in the CFAST prediction is observed due to oscillations in the heat flux calculation (see Figure 11) as discussed above. Figure 15 shows a comparison of the surface temperature of the concrete block predicted by CFAST and measurement. CFAST significantly over-predicts the temperature with an uncertainty of + 128 %. Figure 16 shows a comparison of the front surface temperature of the steel plate predicted by CFAST with measurement. CFAST significantly over-predicts the temperature with an uncertainty of + 111 %.

There were convergence issues in the CFAST simulation of Test 3. The simulation halted at about 14 % to completion. CFAST is sensitive in cases with a high heat flux. The penetration of the thermal wave in the compartment floor and in less dense materials with low thermal conductivity poses numerical challenges for the CFAST code causing the simulation to halt before the end of the transient.

Although the CFAST model could be used to compute global parameters for scenarios like Test 1, its use is limited and not recommended for computing heat fluxes and target responses due to the limitations noted above. For tests more severe than Test 1, the two zone approximation and inherent weaknesses in the code limits its applications. The CFAST model is unsuitable for these scenarios with intense fire sources.

4.2.2 Heat Flux Models in CFAST and FDS

The limitations of the heat flux models in CFAST were discussed above making the model unsuitable for simulating fire scenarios with intense fire sources.

The following provides a summary of the accuracy of the heat flux predictions by FDS. For Test 1, Figure 11 shows a comparison of the total heat flux predicted by FDS with measurements at WS4 on the aerated concrete block. The uncertainty of FDS for total heat flux at WS4 at ~ 40 kW/m2 is + 48 %. Figure 12 shows a comparison of the total heat flux predicted by FDS with measurements at WS3 on the concrete block. The FDS prediction is similar to that measured with an uncertainty of + 14 %. Figure 13 shows a comparison of the total heat flux predicted by FDS with measurements at WS2 on the steel plate. The uncertainty in the FDS prediction is + 59 %. Figure 18 shows a comparison of the heat flux on the wall predicted by FDS with experiment. FDS under predicts the heat flux by - 45 %. The experimental values of the heat flux at WS1 and WS3 which are in comparable locations are similar. Although the FDS prediction for heat flux at WS3 was similar to experiment, it under predicts the flux at WS1.

For Test 3, Figure 32 shows a comparison of the total heat flux predicted by FDS with measurement at WS4 on the aerated concrete block. There is a large increase in heat flux at ~ 1155 s when the HRR reaches its peak at 6000 kW. The uncertainty of the FDS prediction at WS4 at ~ 71 kW/m2 is - 53 %. Figure 33 shows a comparison of the total heat flux predicted by FDS with measurement at WS3 on the concrete block. The uncertainty in the FDS prediction at 66 kW/m2 is - 40 %. Figure 34 shows a comparison of the total heat flux predicted by FDS with measurement at WS2 on the steel plate. The uncertainty in the FDS prediction at 46 kW/m2 is - 23 %. Figure 39 shows a comparison of the heat flux on the wall predicted by FDS with experiment. FDS under predicts the heat flux by - 8 %.

Generally, the error of the heat flux predictions by FDS are large, upto 59 %. There are specific weaknesses in the heat flux models in FDS which make it unreliable for predicting heat fluxes to NPP targets.

4.2.3 Plume Model in FDS

For Test 1, Figure 5 shows an isosurface of the mixture fraction (at a value of 0.062) at 238 s which represents the flame sheet created by FDS at that point. Figure 5 shows that FDS simulates the flame sheet to be significantly pushed toward the rear wall by the flow of ambient air into the compartment through the door. Figure 6 shows a slice profile (at x = 1.8 m) of the gas temperature in the compartment. Figure 6 again shows that FDS simulates that the plume is pushed significantly toward the rear wall.

Figure 7 shows the comparison of measured plume temperatures at M2, M4, and M6 with that predicted by FDS. As shown in Figure 7, FDS predicts peaks in the plume temperature at ~ 50 s. These peaks are explained by the plume development predicted by FDS. Observations of the plume predicted by FDS through Smokeview (the graphical interface for FDS) indicates a steady vertical plume until ~ 50 s when the plume is pushed to the rear wall by flow into the compartment through the door. This causes peaks in the thermocouples, M2, M4, and M6 which are located directly above the fuel pan. The experimental measurements do not indicate this extensive movement of the fire plume. Figure __ shows a photograph of the fire and plume at steady state conditions in Test 1 [need to request Word file from GRS]. The figure shows some degree of plume tilt in the experiment, but not to the extent predicted by FDS. The measured data shows the plume to be fully developed at ~ 105 s after which the plume temperatures increase to ~ 1000 C without any intermediate peaks. The experimental data shows oscillations in the plume temperature, especially near the fire at M2, indicating oscillation of the fire plume to and from the rear wall. FDS predicts the peaks of the plume temperatures to be ~ 800 C. As shown in Table 1, the uncertainty in the predicted values are - 27 %, - 16 %, and - 25 % for M2, M4, and M6, respectively.

Figure 8 shows the local gas temperatures in the compartment at Level 1 for M7, M8, M9, and M10. The measured temperatures show a rapid increase in temperature followed by a more gradual increase until the end of the transient. The temperature measured at M10 is much higher than that measured at M7, M8, and M9. This is due to the tilting of the fire plume toward M10. FDS also shows a rapid increase in temperature followed by large oscillations and unexpected trends. These oscillations may be caused by oscillations in the flow through the door predicted by FDS. The temperature predicted at M8 by FDS is highest since the code predicts the fire plume to be pushed more toward the rear wall, as discussed above. The experimental data shows some oscillations in the temperature at M10 indicating the movement of the plume in and out of that region. Although the peak values predicted by FDS are similar to that measured for M7, M8, and M9, there is an uncertainty of - 43 % for M10 due to the discrepancy in the degree of plume tilt predicted.

Similar observations were made for the results of Test 3 and are discussed in section 3.2.2 in Chapter 3. FDS computations of the plume predict a larger tilt due to flow conditions, whereas, the plumes in the experiments are observed to be stiffer and influenced less by flow conditions. This limits the reliability and accuracy of using FDS to evaluate targets near the plume.

4.2.4 Target Models in CFAST and FDS

A detailed heat transfer model for the barrel used in the experiments will be fairly complex. The CFAST and FDS fire models are not capable of modeling complex configurations such as the barrel for storing radioactive waste. The cylindrical geometry and multi-material composition poses challenges for modeling. Similar limitations of CFAST and FDS for modeling cable targets were noted in ICFMP Benchmark Exercise # 1 [Dey, 2002].

The limitations and large uncertainties for predicting the temperature of the material probes with CFAST was discussed above. Although the predictions of heat fluxes by FDS have large uncertainties (up to 59 %), the temperature predictions for the material probes for Test 1 are fortuitously better, but larger for Test 3 (-33 %). The large uncertainties in the prediction of heat flux to the targets limit the reliability of using FDS or CFAST for predicting target temperatures. Lack of ability to model targets other than rectangular slabs, e.g. radioactive waste barrels, limit the usefulness of the codes for NPP target analysis.

4.2.5 Extinction Models in FDS and CFAST

The flow of ambient air through the door in Test 1 provided the fire with full ventilation throughout the transient. The CFAST code was not even capable of modeling Test 3, so its limitations for predicting the under ventilation of the fire in Test 3 is not discussed.

Figure 26 shows a slice profile (at x = 1.8 m, t = 101.5 s) of the gas temperature in the compartment. Figure 27 shows a slice profile (at x = 1.8 m, t = 102 s) of the gas temperature in the compartment. Observations of this temperature slice file in Smokeview shows that FDS simulates the flow through the door to pulsate with a period of ~ 2 s. Figure 26 shows the flow through the door to be bidirectional, whereas Figure 27 shows the end of the cycle of the pulsation when the flow is unidirectional through the door flowing out of the compartment. This pulsating behavior was noted during the experiments and is mentioned in Klein-Hessling, 2005. The pulsating flow through the door provides sufficient oxygen to the fire and prevents it from being under ventilated. Although fluid dynamics of the scenario is simulated well by FDS, the simple extinction model in FDS (LOL) decreases the heat output from the fire when combustion is fully sustained. The discrepancy in the HRR from FDS and measured is shown in Figure 20. The algorithm in FDS for accounting for the under ventilation of the fire is too simplistic for complex scenarios as in this benchmark exercise.

4.2.6 Modeling of Multi-Layer Boundaries with CFAST and FDS

The CFAST and FDS codes do not have the capability to model multi-layer boundaries, therefore, a single-layer assumption had to be adopted to model the aerated concrete around the fuel pan and the concrete floor below. The layer of insulation covering the walls and ceiling was neglected in the calculations since it could not be directly modeled in CFAST or FDS. Further, the multi-layer composition of the target barrel could not be modeled, although the modeling of the cylindrical geometry is a more fundamental limitation. The use of these codes for complex target geometries and composition is very limited.

4.3 User Interface

<u>FDS</u>

The FDS manuals (Technical Reference Guide and User’s Guide), in conjunction with the Smokeview graphical interface for reviewing results of the computations, provide a useful interface for the user. The quality of this interface has positively impacted the capability to analyze and interpret the predicted results.

<u>CFAST</u>

Although the Technical Reference Guide for CFAST is detailed, its relationship to the User’s

Guide, and a useful and comprehensive User's Guide is lacking. Additionally, the graphical user interface (GUI) for CFAST is outdated and does not function in more recent operating platforms such as Windows XP. It would be beneficial to have a comprehensive User's Guide and enhanced GUI to allow more accurate input of data for the simulations and understanding of output parameters such as their units.

The users of these codes should be knowledgeable of the complexities of the compartment conditions, such as plume movement, to assess and utilize the results of their calculations.

4.4 Benefits of Hand Calculations

In order to evaluate the benefits of hand calculations, Specified Calculations with FDTs [NRC, 2004] were conducted and submitted to GRS. GRS has certified the authenticity of these Specified Calculations. The results of the calculations are compared with experimental data for Test 1 and shown in Table 3 below. The comparisons show that hand calculations could provide a method to quickly calculate global parameters (HGL temperature and interface height), as well as plume temperatures using simple correlations. Some large deviations for heat fluxes (-66 %) and plume temperature at M6 (-66 %) are noted. The heat flux correlations used may not have had a large fire, such as the one in Test 1, included in the development of the correlation. Also, the plume correlation is for erect plumes and not when the fire plume is tilted, as is evident from the uncertainty at M6. Since the range of validity of the correlations is narrow, the results are best suited for a screening calculation where a rough estimate is required, while acknowledging the answers may contain large inaccuracies.

4.5 Need for Model Improvements

<u>CFAST</u>

The CFAST model requires major fundamental improvements if it is to be used for fire scenarios with intense fire sources such as those examined in this benchmark exercise. The computation of thermal propagation through materials with low density and conductivity should be reviewed to determine if this limitation can be solved and eliminated. Further, an examination should be conducted to determine whether the computational limitation for simulating Test 3 is inherent in the code, or whether it can be addressed with improvements to the numerics in the code.

<u>FDS</u>

Although relatively good general performance is noted above, the heat flux models (for radiation and convection) in FDS require improvement before they can be reliably used for NPP applications. The target model also requires improvement to analyze NPP targets. The code should also be improved to accurately simulate plume behavior and tilting due to varying flow conditions in the compartment. For Test 3, the HRR used by FDS was less than input for the simulation due to algorithms in FDS to account for under ventilated conditions. These algorithms should be corrected to maintain the HRRs prescribed by the user to improve the performance and accuracy of the model. The basic extinction phenomena requires a more fundamental treatment in FDS to be able to predict under ventilated conditions. Finally, the ability simulate multi-layer boundaries and targets needs to be implemented in FDS for NPP applications.

The prediction of burning rate is an important area of research that is being conducted at NIST. This research was investigated by NIST through exercising FDS for specified calculations for this benchmark exercise (see Appendix _ in Klein-Hessling, 2005). The investigation concluded that the prediction of burning rate was challenging. The analyst was required to supplement the given fuel properties with values from the literature which results in large uncertainties in the simulation. Given the uncertainties, the results should only be used to assess the qualitative behavior of the phenomena. More research and validation work is needed before the model can be used to reliably predict burning rate of liquid fuels, especially in under ventilated compartments. Validation work should focus on the fire and the fuel bed. FDS requires improvements in the near field. In addition to the measurement of burning rate, measurements are needed to measure the heat flux and temperature at the fuel surface, and the thermal and chemical environment of the fire itself. Boundary and geometrical effects should be minimized by using solid homogenous slabs or liquid pools.

4.6 Need for Advanced Models

As discussed above, zone models are limited for simulating the severe thermal environments in the test scenarios of this Benchmark Exercise. CFD codes, such as FDS, inherently include more physics of the phenomena in the compartment that allow them to be less limited and more accurate in simulating parameters of interest for NPP applications of such scenarios.

The computational requirements for CFD codes should be noted. The tests in this benchmark exercise required 70 to 160 hours to compute with FDS, whereas, zone models can be executed in less than 10 s.

4.7 Need for Additional Test Programs

The two test scenarios for Benchmark Exercise # 4 provide a useful and complete data set for assessing the capabilities of fire models for extreme compartment fire conditions for NPP applications. Other tests were conducted in the series which could also be used for further evaluations. It may be useful to use data from these other tests to evaluate performance of the codes for predicting CO and CO_2 concentrations as these data were not available for Tests 1 and 3.

These tests provide fire scenarios with intense fire sources in a compartment. It will be beneficial to conduct tests that provide a range of fire intensities so that one can determine the limits of zone models over which their theoretical formulations remain valid.

References

American Society of Testing and Materials, “Evaluating the Predictive Capability of Deterministic Fire Models,” ASTM E1355-04, West Conshohocken, PA (2004).

Dey, M ., Ed., “Evaluation of Fire Models for Nuclear Power Plant Applications,” U.S. Nuclear Regulatory Commission, NUREG-1758, Washington DC, USA, June 2002.

Jones, W., Ed., “CFAST - Consolidated Model of Fire Growth and Smoke Transport (Version 5), National Institute of Standards and Technology, NIST Special Publication 1030, October 2004.

Klein-Hessling, W., “Evaluation of Fire Models for Nuclear Power Plant Applications: Large Pool Fires in a Compartment,” to be published.

McGrattan, K., Ed., “Fire Dynamics Simulator (Version 4), Technical Reference Guide,” National Institute of Standards and Technology, NIST Special Publication 1018, September 2004.

Miles, S. Ed., “Evaluation of Fire Models for Nuclear Power Plant Applications: Pool Fires In Large Halls,” Building Research Establishment, BRE Report No. 212214, May 2004, Watford, UK.

Society of Fire Protection Engineers, “The SFPE Handbook of Fire Protection Engineering,” 2nd Edition, Bethesda, Maryland, 1995.

U.S. Nuclear Regulatory Commission, " Fire Dynamics Tools (FDTs) Quantitative Fire Hazard Analysis Methods for the U.S. Nuclear Regulatory Commission Fire Protection Inspection Program," NUREG-1805, Washington DC, USA, November 2004.

Table 1 Summary of Predictions with CFAST and FDS for Test 1
Specified Predictions

Parameter	**Sensor**	**Model prediction at peak**		**Measured value at peak**	**Initial measured value**	**Uncertainty**	
		CFAST	**FDS**			**CFAST**	**FDS**
Global Parameters							
HGL Interface Ht		0.7 m	0.7 m	1.5 m	5.7 m	- 19 %	- 19 %
HGL Temp. (Average)		857 C	600 C	719 C	19 C	+ 20 %	- 17 %
O2 Conc.	GA1 O2					NA	NA
Smoke Conc.						NA	NA
CO Conc.						NA	NA
Pressure						NA	NA
Flame Height						NA	NA
Local Gas Temperatures							
Plume Temp.	M 2		768 C	1036 C	19 C		-27 %
	M 4		824 C	971 C	19 C		- 16 %
	M 6		786 C	1040 C	19 C		- 25 %
Hot Gas Temp. (point values)	M 10		464 C	800 C	19 C		- 43 %
	M 14		660 C	753 C	19 C		- 13 %
	M 18		684 C	722 C	19 C		- 5 %
Ceiling Jet Temp.	M 18		684 C	722 C	19 C		- 5 %
Target Heat Flux and Temperature							
Radiative Heat Flux to Cables						NA	NA
Total Heat Flux to Cables						NA	NA
Cable Surface Temp.						NA	NA

Total Heat Flux to Plates/Blocks	WS 2	85 kW/m2	43 kW/m2	27 kW/m2	0	+ 215 %	+ 59 %
	WS 3	86 kW/m2	40 kW/m2	35 kW/m2	0	+ 146 %	+ 14 %
	WS 4	NA	40 kW/m2	27 kW/m2	0	NA	+ 48 %
Plates/ Blocks Surface Temp.	M 29	NA	595 C	504 C	19 C	NA	+ 19 %
	M 33	715 C	409 C	325 C	19 C	+ 128 %	+ 28 %
	M 34	770 C	400 C	375 C	19 C	+ 111 %	+ 7 %
Wall Flux and Temperature							
Total Heat Flux to Walls	WS 1		16.6 kW/m2	30 kW/m2	0	NA	- 45 %
Wall Surface Temp	M 20		735 C	589 C	19 C		- 26 %

Notes:
+ Model prediction was greater than measured value
- Model prediction was less than measured value
Value tabulated is: (model prediction at peak- measured value at peak)/(measured value at peak - initial measured value)

Table 2 Summary of Predictions with CFAST and FDS for Test 3
Specified Predictions

Parameter	**Sensor**	**Model prediction at peak**		**Measured value at peak**	**Initial measured value**	**Uncertainty**	
		CFAST	**FDS**			**CFAST**	**FDS**
Global Parameters							
HGL Interface Ht			0.6 m	1.6 m	5.7 m		- 24 %
HGL Temp. (Average)			662 C	961 C	19 C		- 32 %
O2 Conc.	GA1 O2						- 25 %
Smoke Conc.							NA
CO Conc.							NA
Pressure							NA
Flame Height							NA
Local Gas Temperature							
Plume Temp.	M 2		774 C	1036 C	19 C		-26 %
	M 4		811 C	971 C	19 C		- 17 %
	M 6		774 C	1041 C	19 C		- 27 %
Hot Gas Temp. (point values)	M 10		628 C	921 C	19 C		- 33 %
	M 14		692 C	906 C	19 C		- 24 %
	M 18		707 C	966 C	19 C		- 27 %
Ceiling Jet Temp.	M 18		715 C	966 C	19 C		- 27 %
Target Heat Flux and Temperature							
Cable Surface Temp.							NA
Radiative Heat Flux to Cables							NA
Total Heat Flux to Cables							NA

Total Heat Flux to Plates/Blocks	WS 2		46 kW/m2	60 kW/m2	0		- 23 %
	WS 3		66 kW/m2	110 kW/m2	0		- 40 %
	WS 4		71 kW/m2	150 kW/m2	0		- 53 %
Plates/ Blocks Surface Temp.	M 29		712 C	698 C	19 C		+ 2 %
	M 33		387 C	565 C	19 C		- 33 %
	M 34		313 C	460 C	19 C		- 33 %
Wall Heat Flux and Temperature							
Total Heat Flux to Walls	WS 1		92 kW/m2	100 kW/m2	0		- 8 %
Wall Surface Temp	M 20		575 C	852 C	19 C		- 34 %

Notes:
+ Model prediction was greater than measured value
- Model prediction was less than measured value
Value tabulated is: (model prediction at peak- measured value at peak)/(measured value at peak - initial measured value)

Table 3 Summary of Predictions with FDTs - Test 1
Specified Predictions

Parameter	Sensor	Model prediction at peak	Measured value at peak	Initial measured value	Uncertainty
Global Parameters					
HGL Interface Ht		0 m @ 60 s	1.5 m	5.7 m	- 36 %
HGL Temp. (Average)		719 C @ 1200 s	719 C	19 C	+ 0 %
Local Gas Temperature					
Plume Temp.	M 2	Out of Range	1036 C	19 C	NA
	M 4	869	971 C	19 C	- 11 %
	M 6	347	1040 C	19 C	- 66 %
Target Heat Flux					
	WS 3	11.7 kW/m2 solid flame w/o wind 16.7 kW/m2 point source	35 kW/m2	0	- 66 % - 53 %
	At barrel	45.8 kW/m2 solid flame with wind, v=2.5 m/s, Angle =48^0	No measurement available.		

Notes:
+ Model prediction was greater than measured value
- Model prediction was less than measured value
Value tabulated is: (model prediction at peak- measured value at peak)/(measured value at peak - initial measured value)

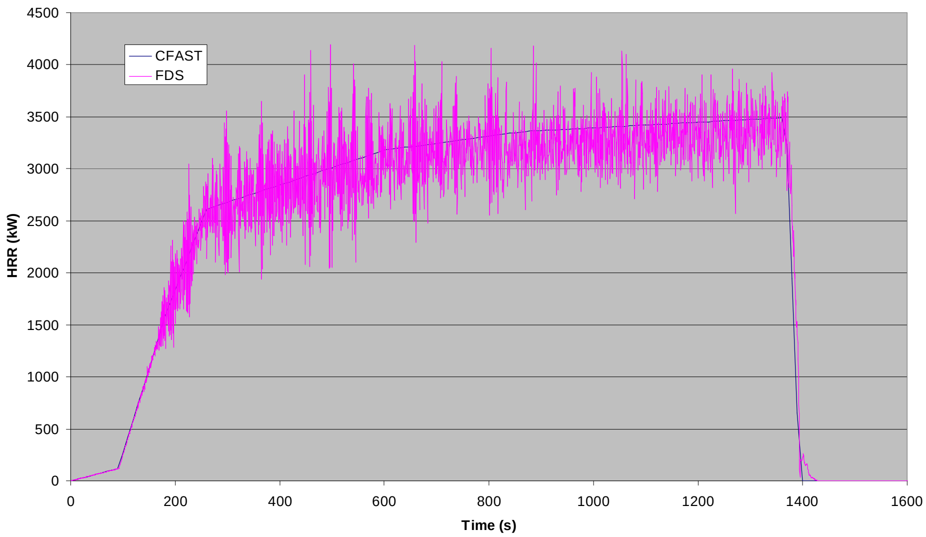

Figure 1 Heat Release Rate - Test 1

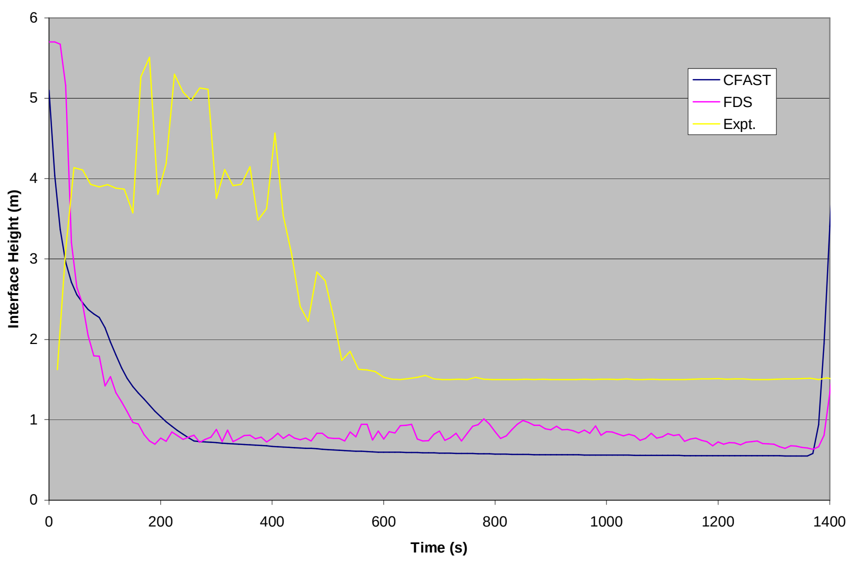

Figure 2 HGL Interface Height - Test 1

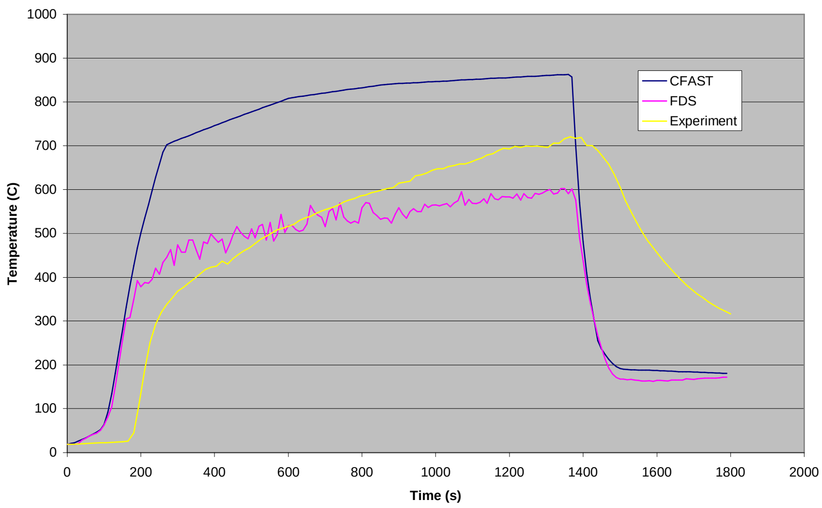

Figure 3 HGL Temperature - Test 1

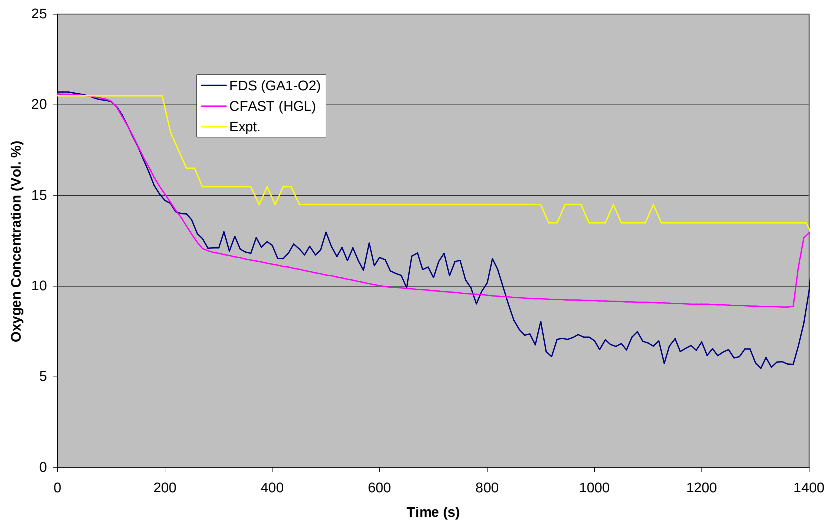

Figure 4 Oxygen Concentration

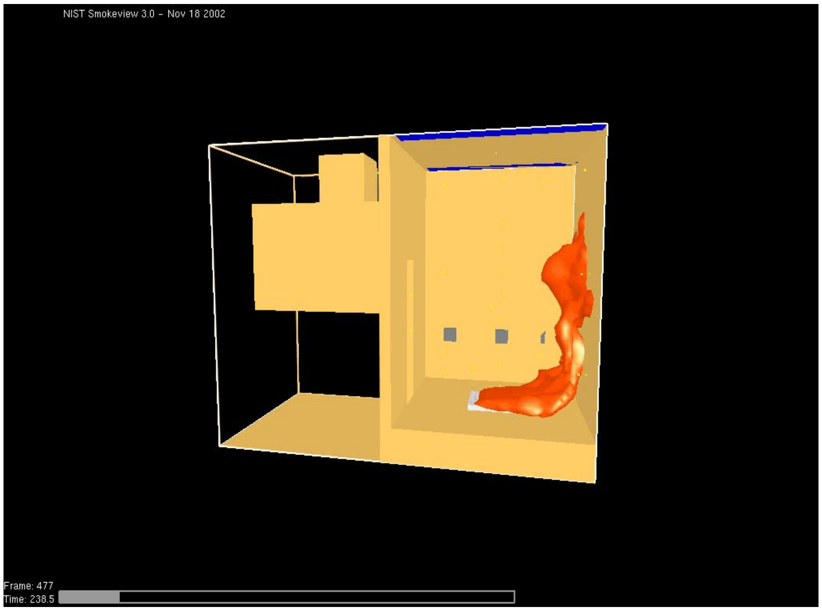

Figure 5 View of Flamesheet Output from FDS - Test 1

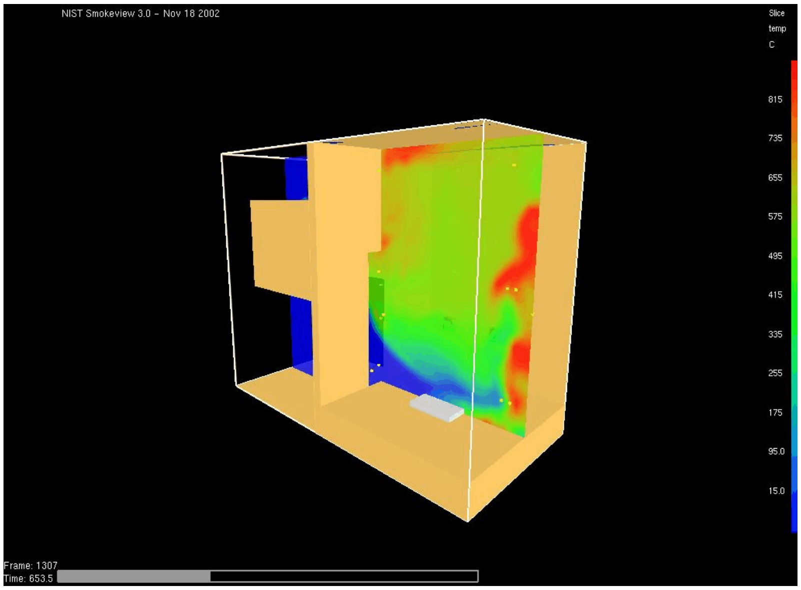

Figure 6 View of Temperature Slice (x=1.8 m) - Test 1

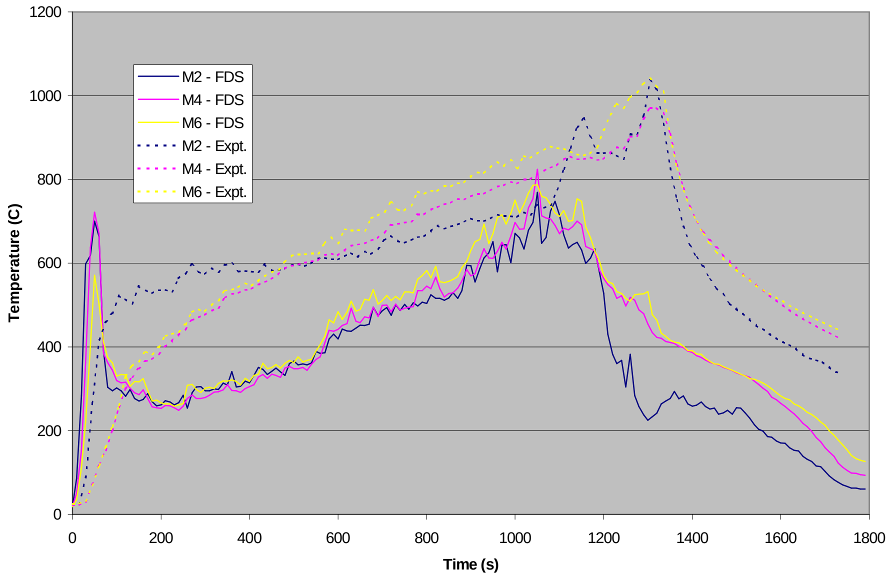

Figure 7 Plume Temperature - Test 1

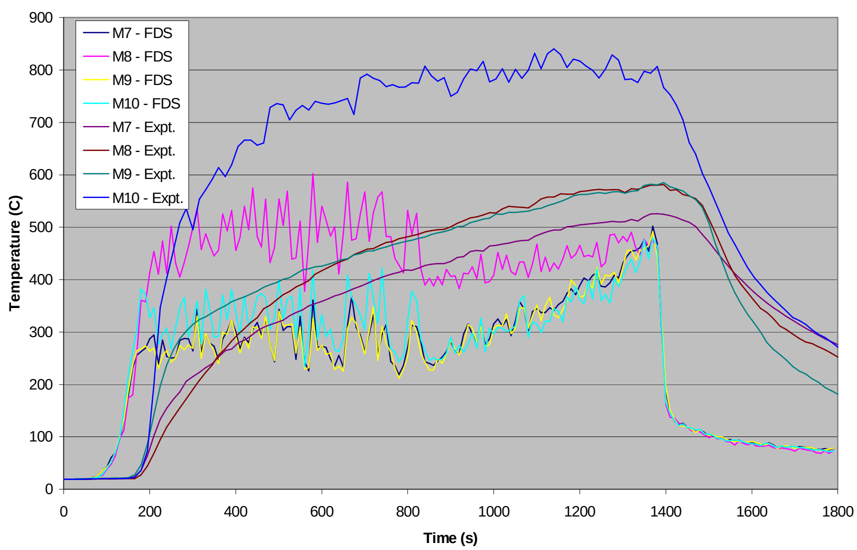

Figure 8 Level 1 Temperatures - Test 1

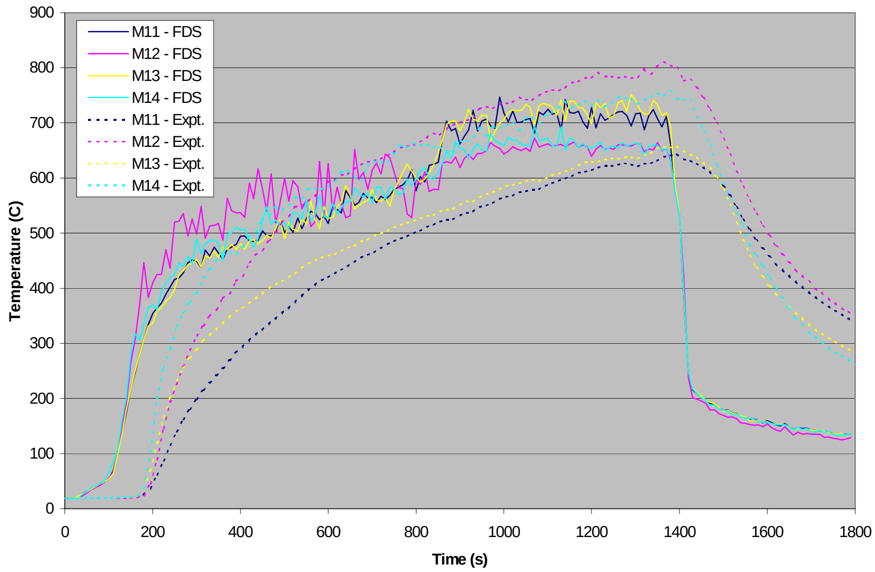

Figure 9 Level 2 Temperatures - Test 1

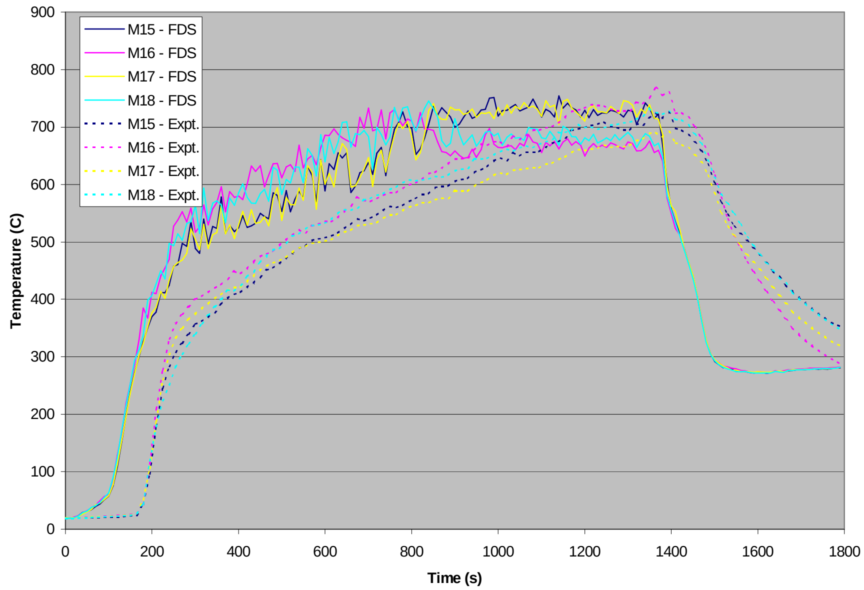

Figure 10 Level 3 Temperatures - Test 1

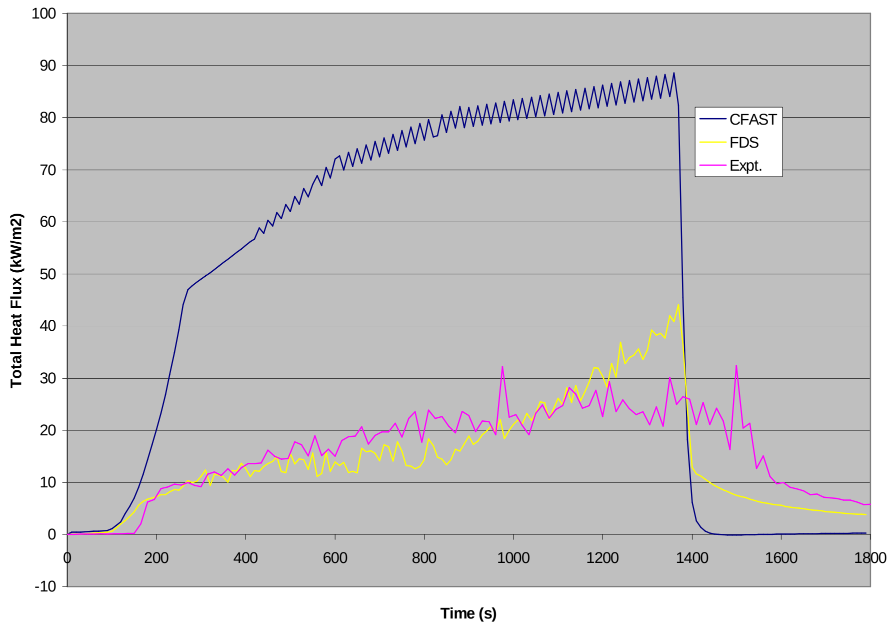

Figure 11 Heat Flux on Aerated Concrete Block (WS4) - Test 1

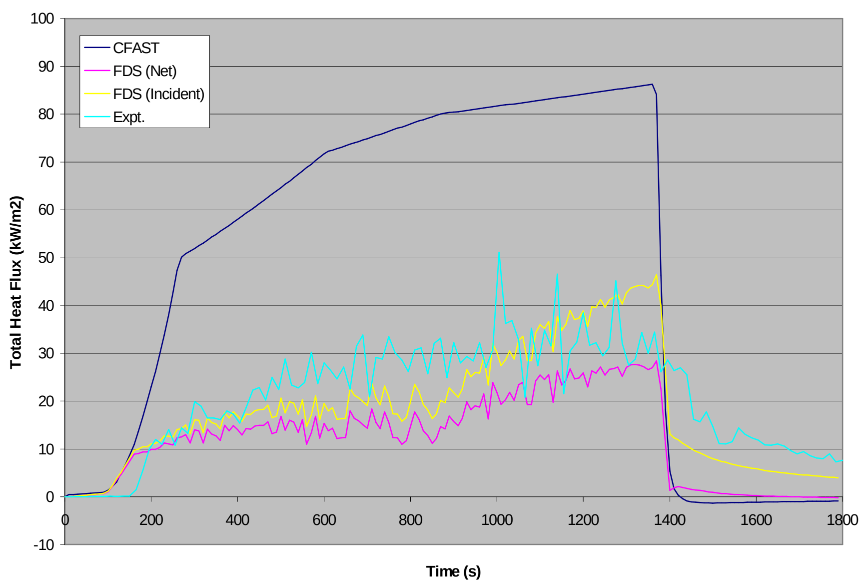

Figure 12 Heat Flux on Concrete Block (WS3) - Test 1

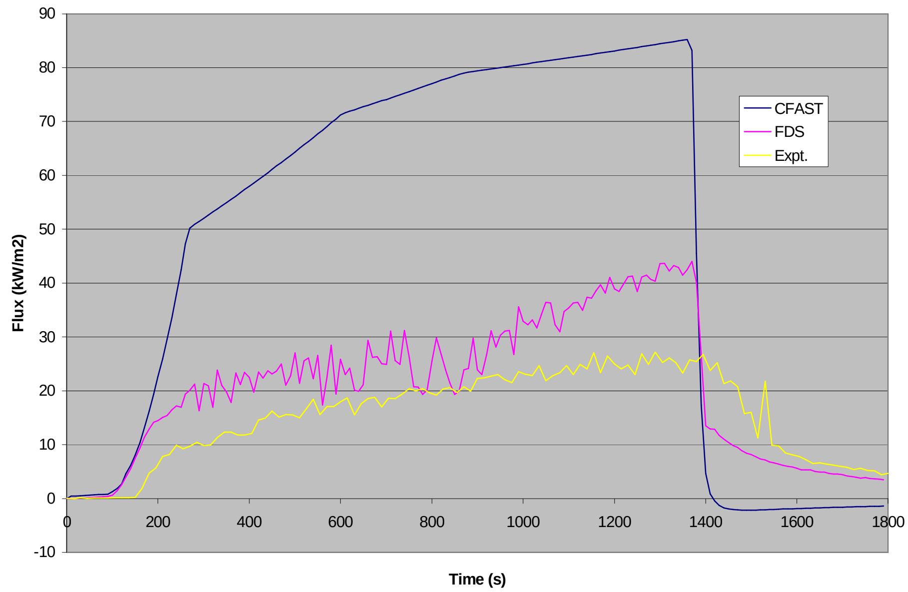

Figure 13 Heat Flux on Steel Plate (WS2) - Test 1

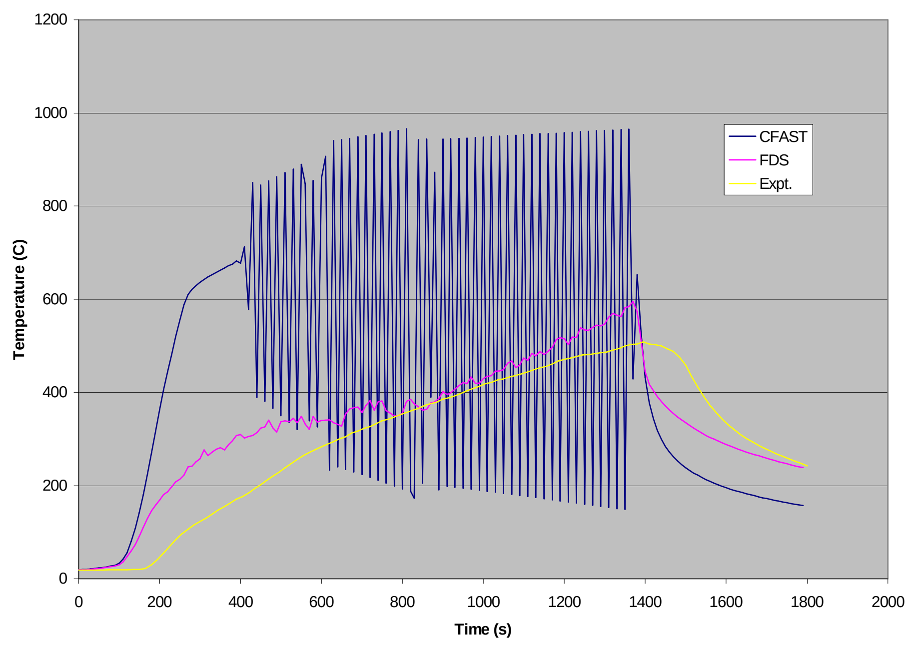

Figure 14 Aerated Concrete Block Temperature - Test 1

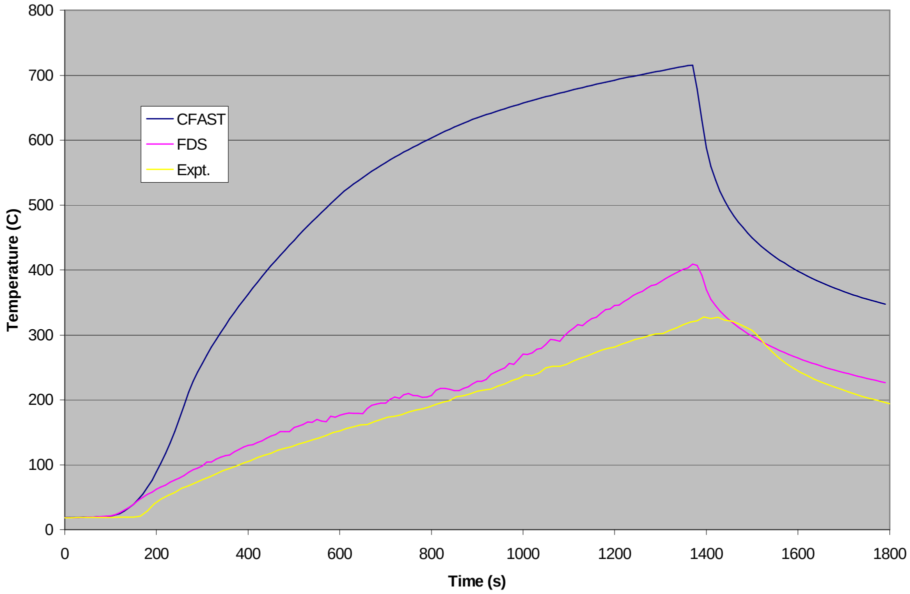

Figure 15 Concrete Block Temperature - Test 1

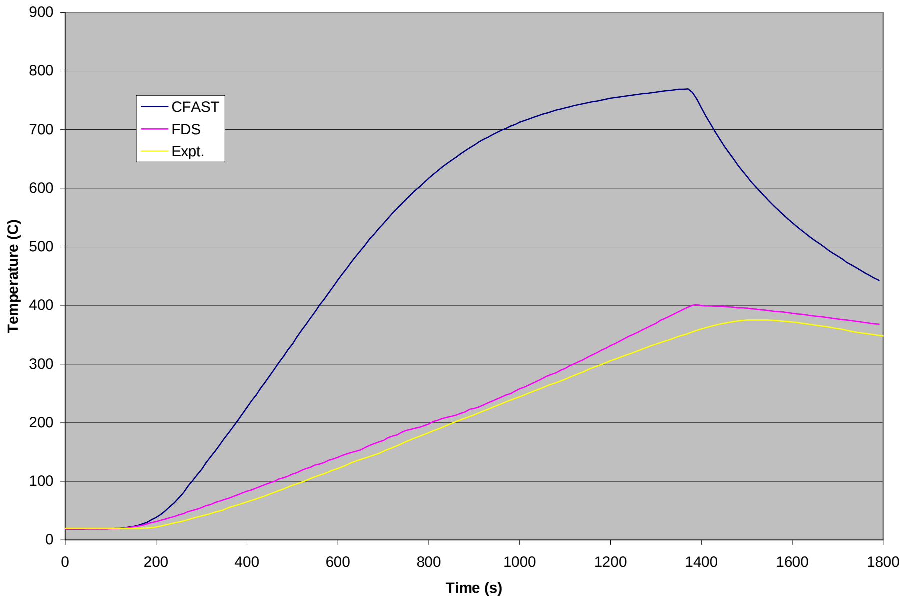

Figure 16 Steel Plate Front Surface Temperature (M34) - Test 1

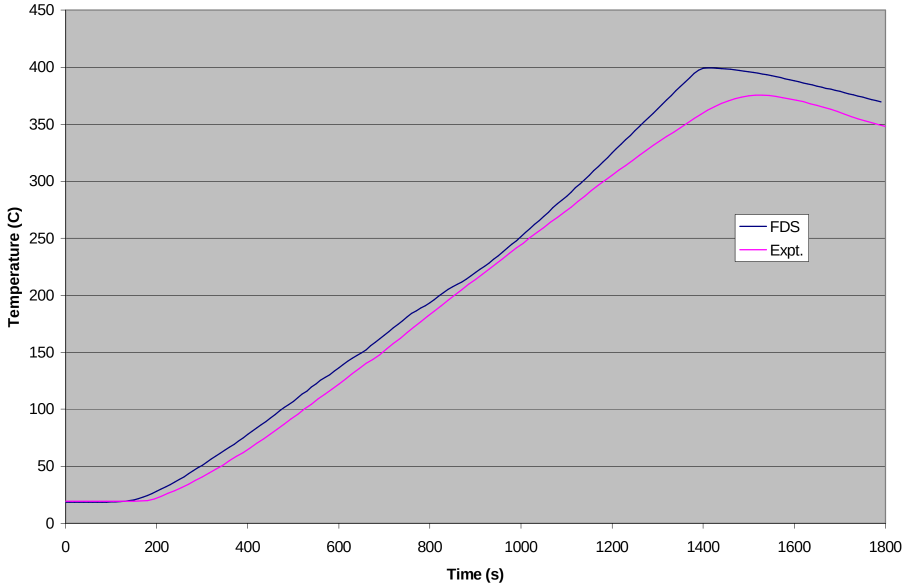

Figure 17 Steel Plate Back Surface Temperature (M35) - Test 1

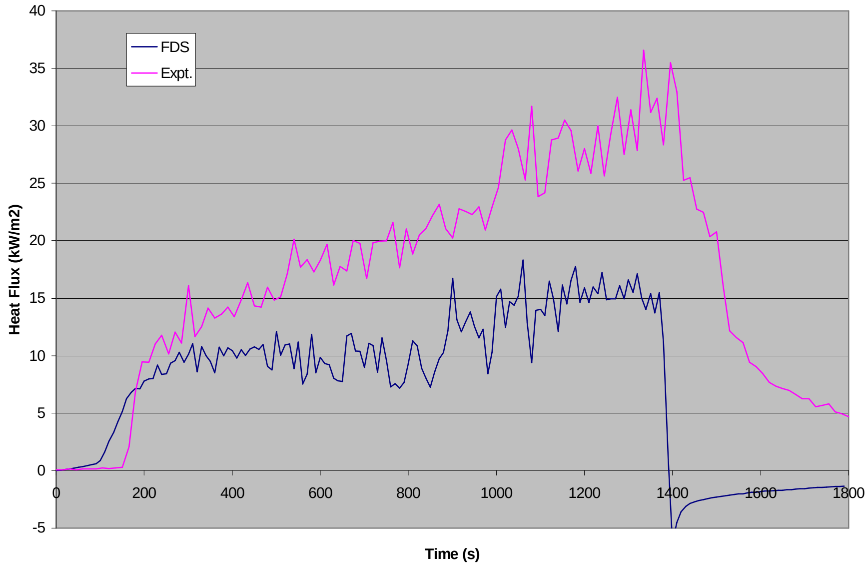

Figure 18 Heat Flux on Wall (WS1) - Test 1

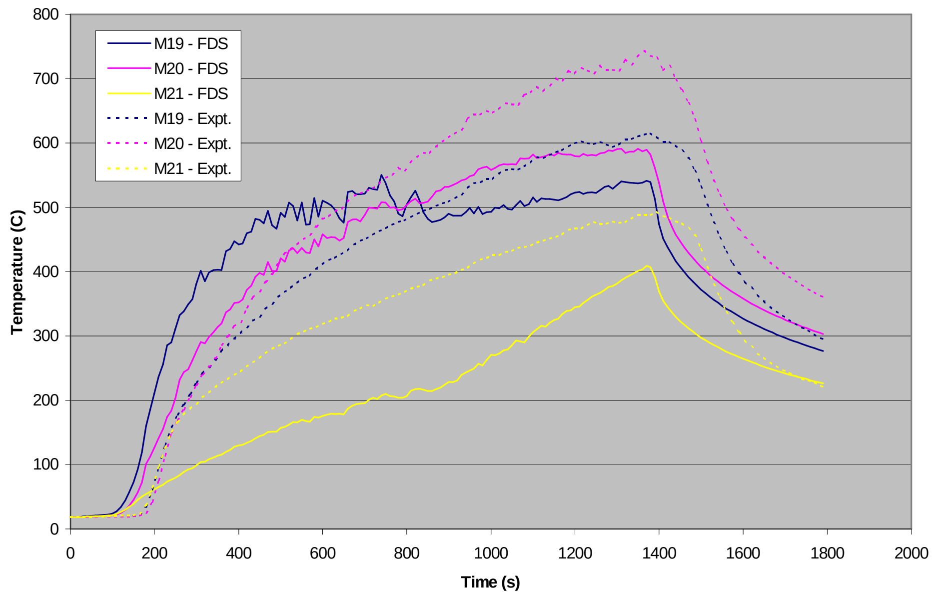

Figure 19 Wall Temperatures - Test 1

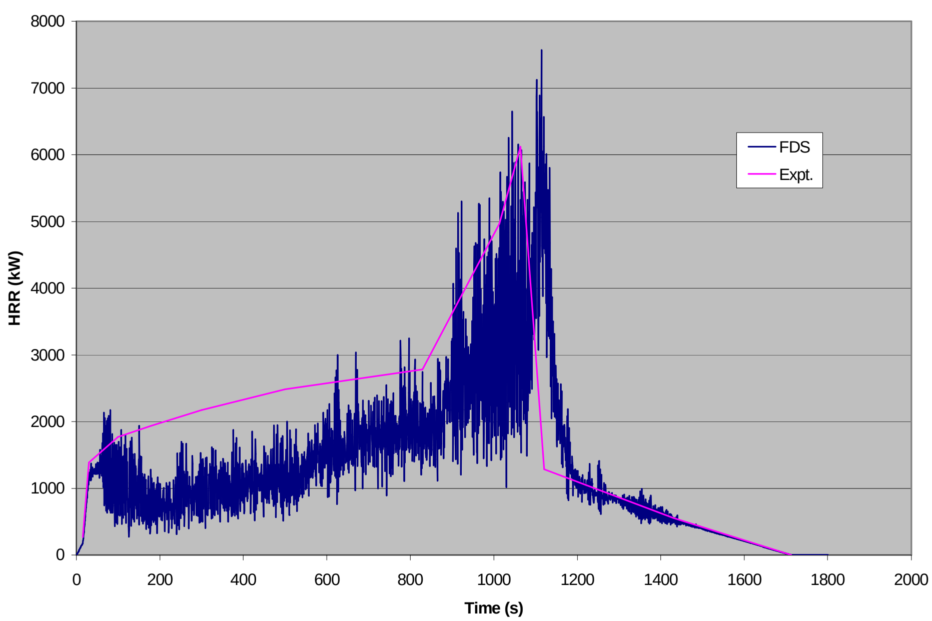

Figure 20 Heat Release Rate - Test 3

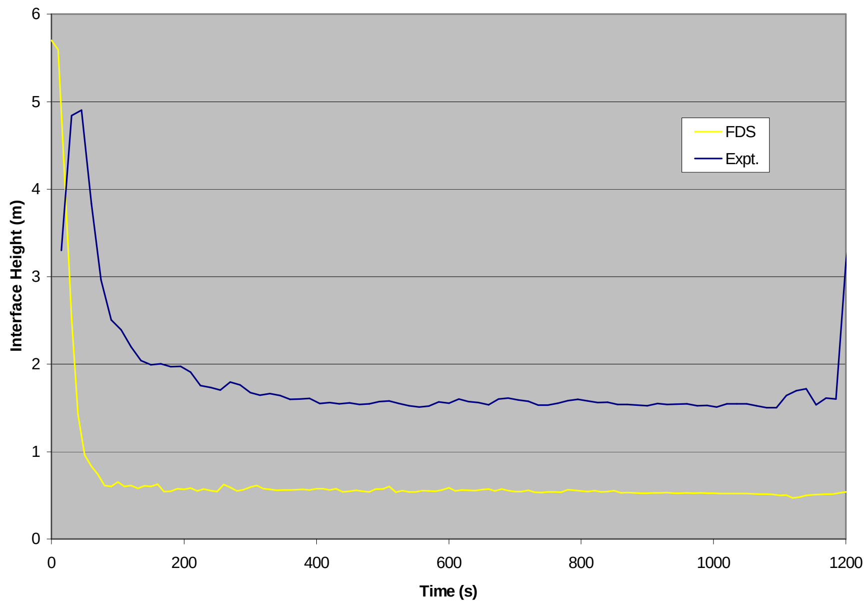

Figure 21 HGL Interface Height - Test 3

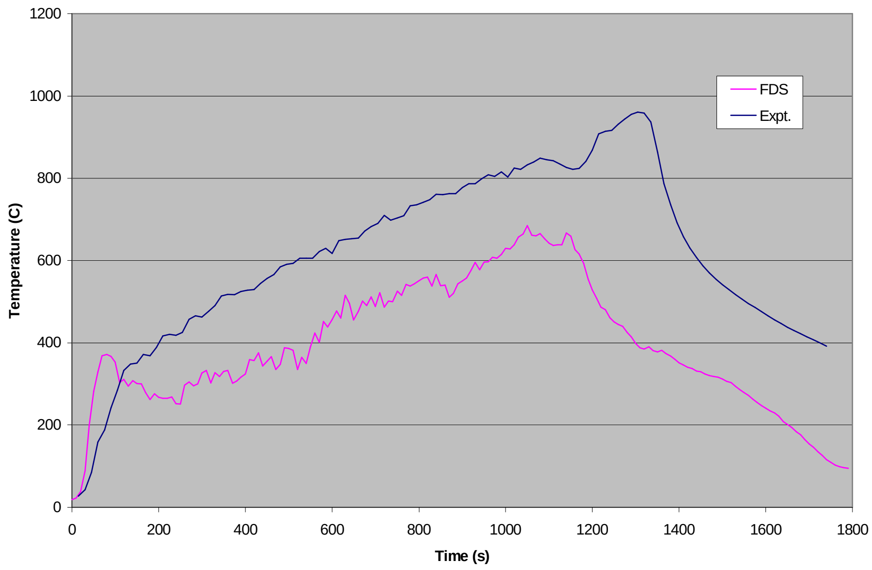

Figure 22 HGL Temperature - Test 3

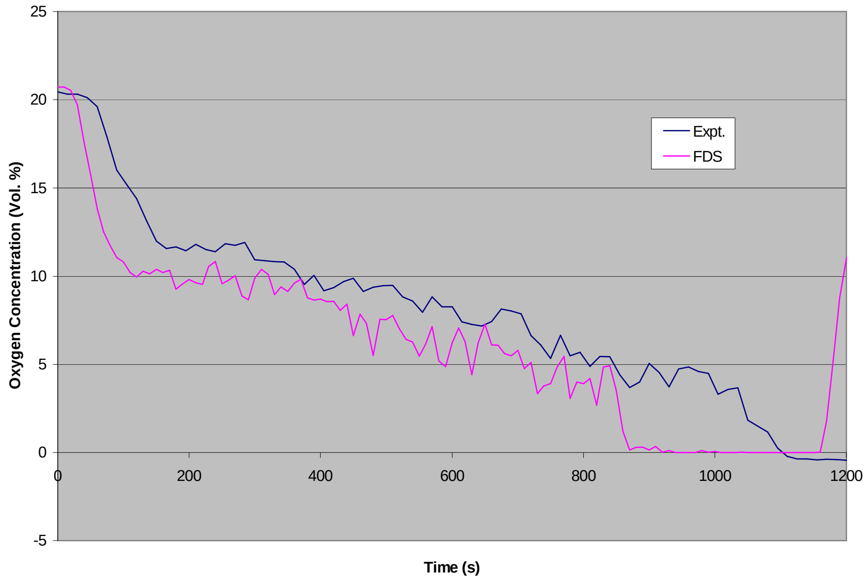

Figure 23 Oxygen Concentration - Test 3

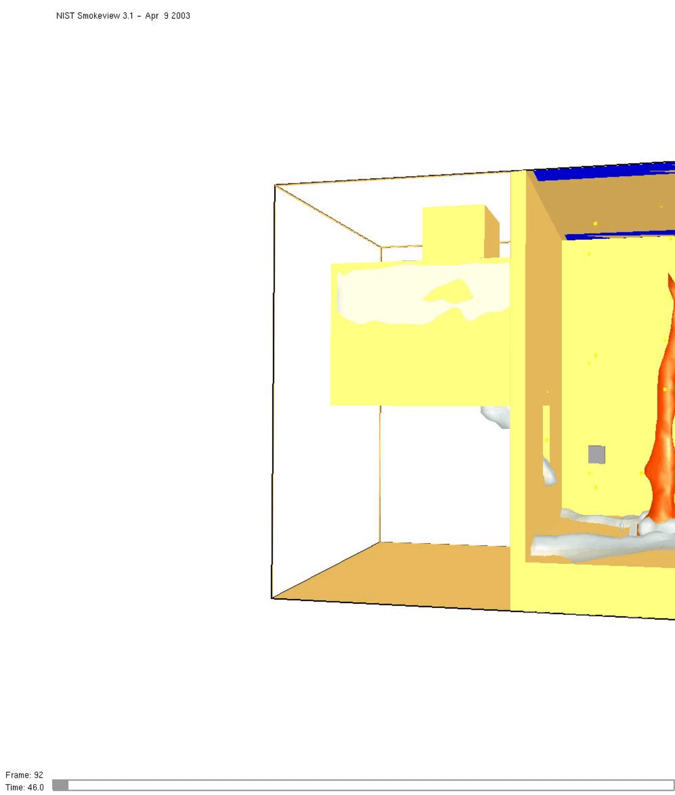

Figure 24 View of Flame Sheet Output from FDS (45 s) - Test 3

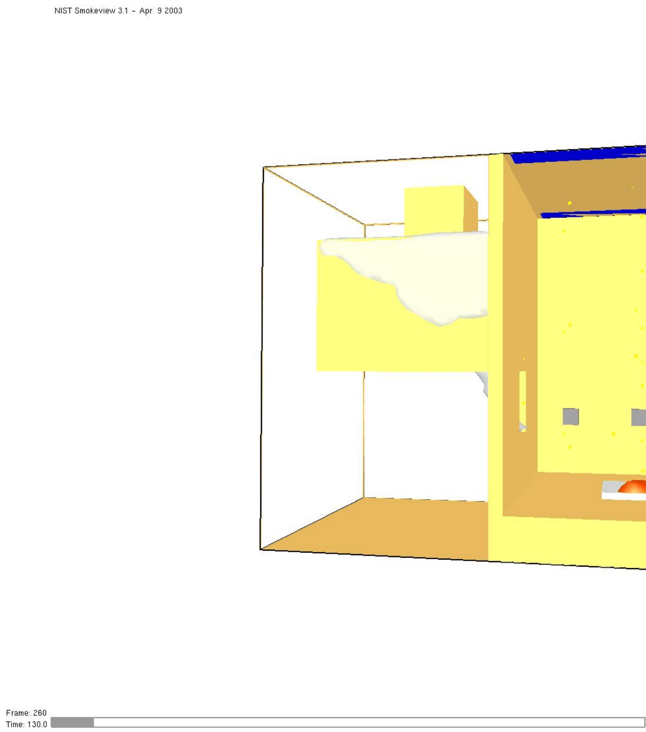

Figure 25 View of Flame Sheet Output from FDS (130 s) - Test 3

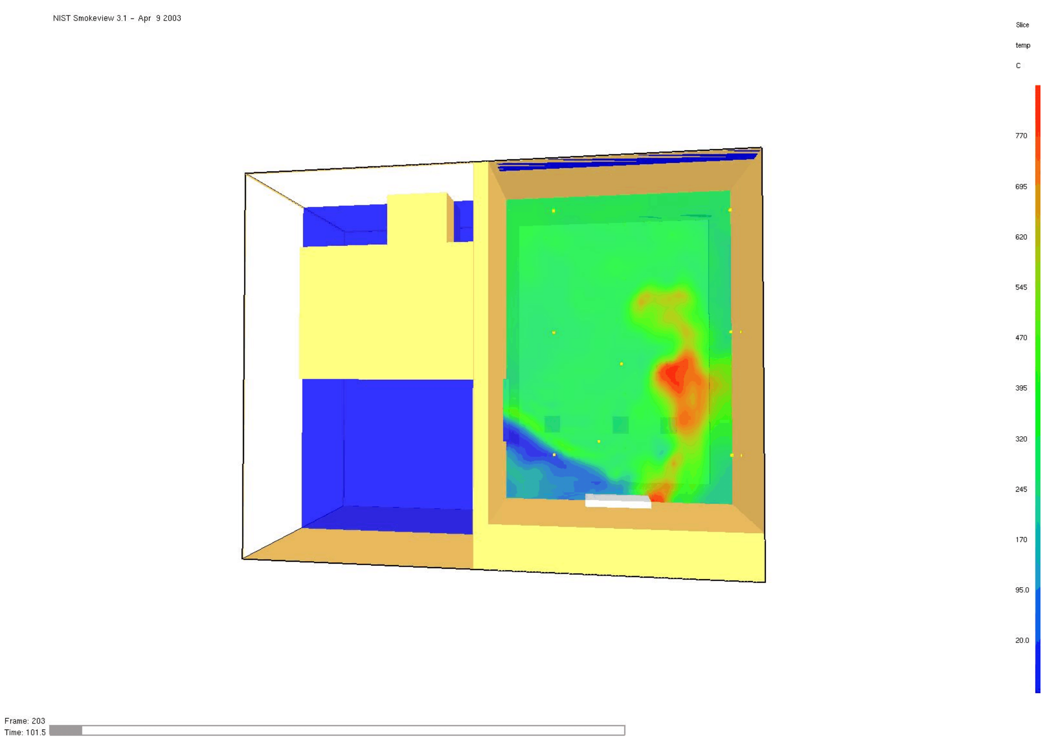

Figure 26 View of Temperature Slice (x=2.8 m, t=101.5 s) - Test 3

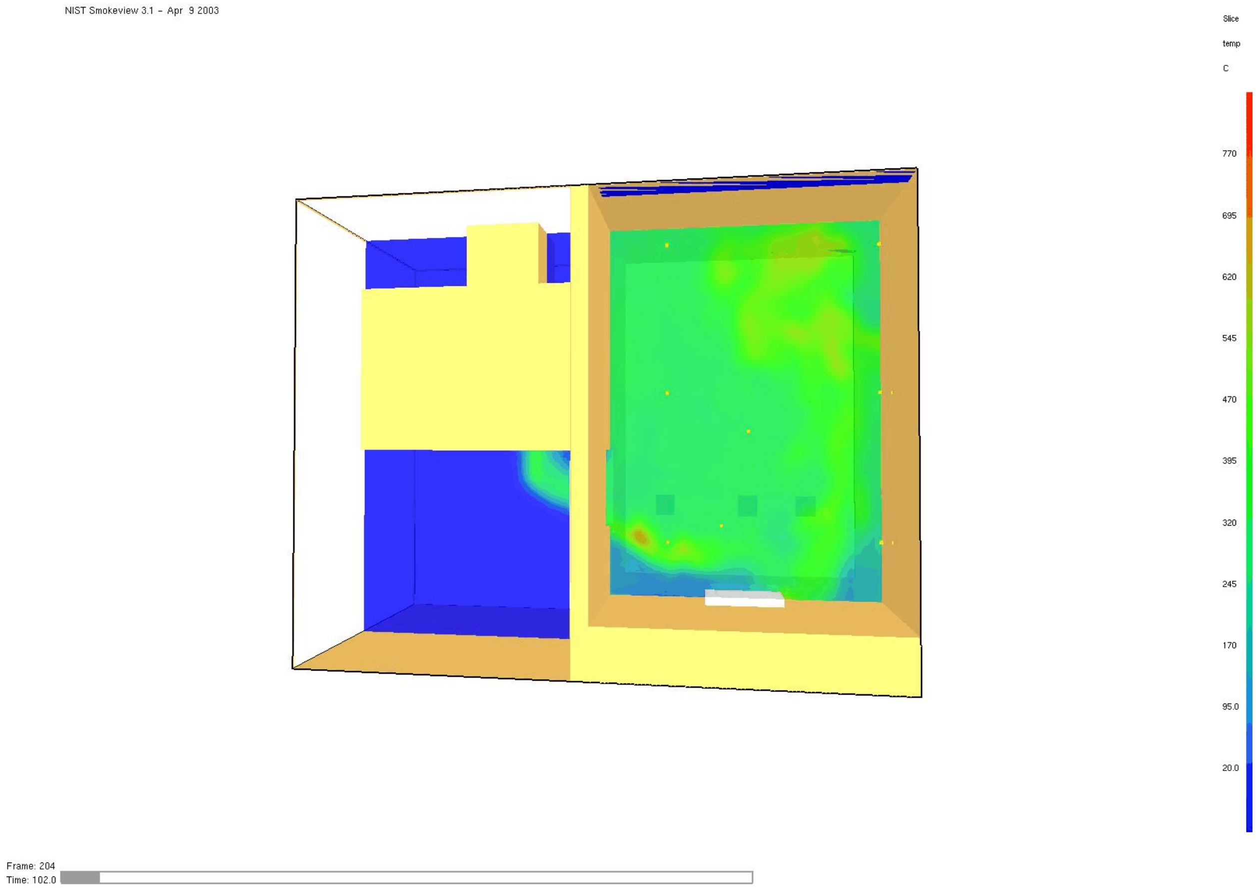

Figure 27 View of Temperature Slice (x=2.8 m), t=102 s) - Test 3

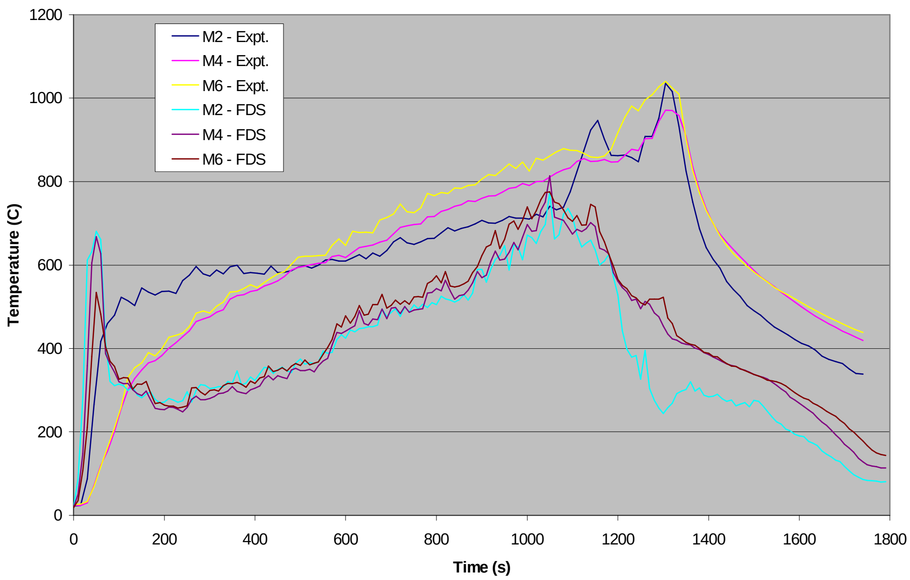

Figure 28 Plume Temperature - Test 3

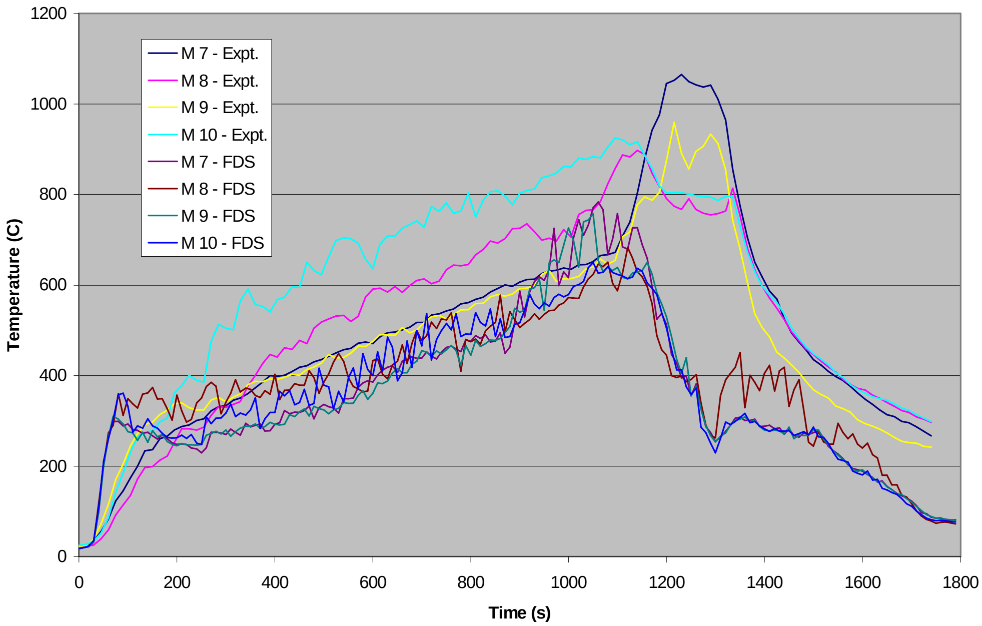

Figure 29 Level 1 Temperature - Test 3

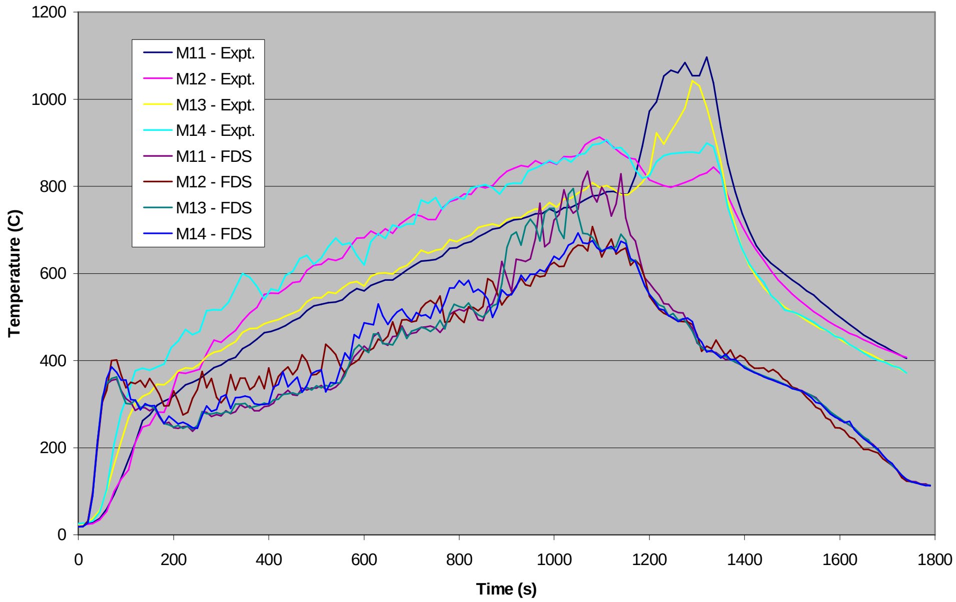

Figure 30 Level 2 Temperature - Test 3

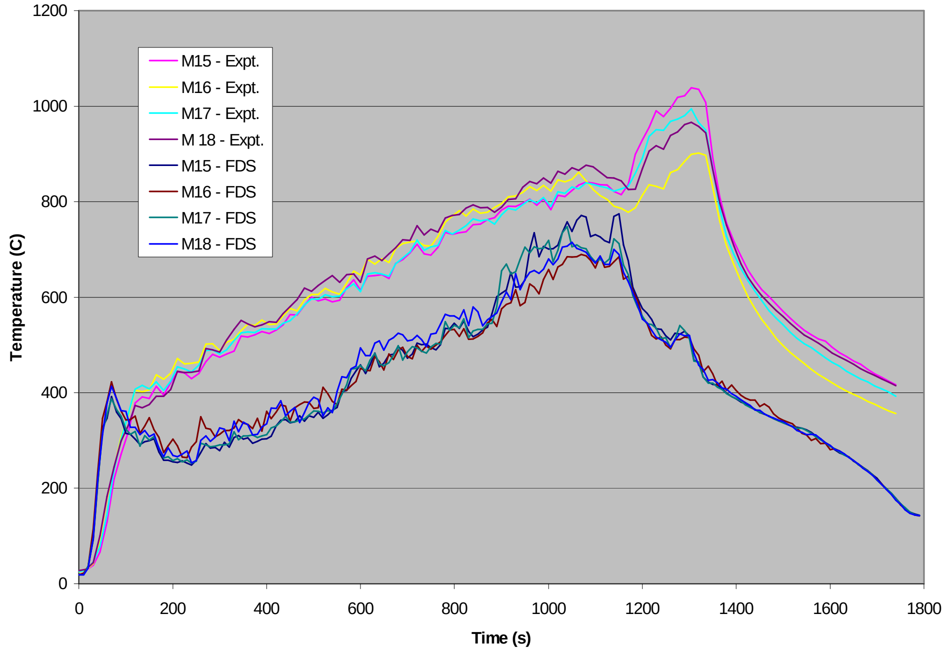

Figure 31 Level 3 Temperature - Test 3

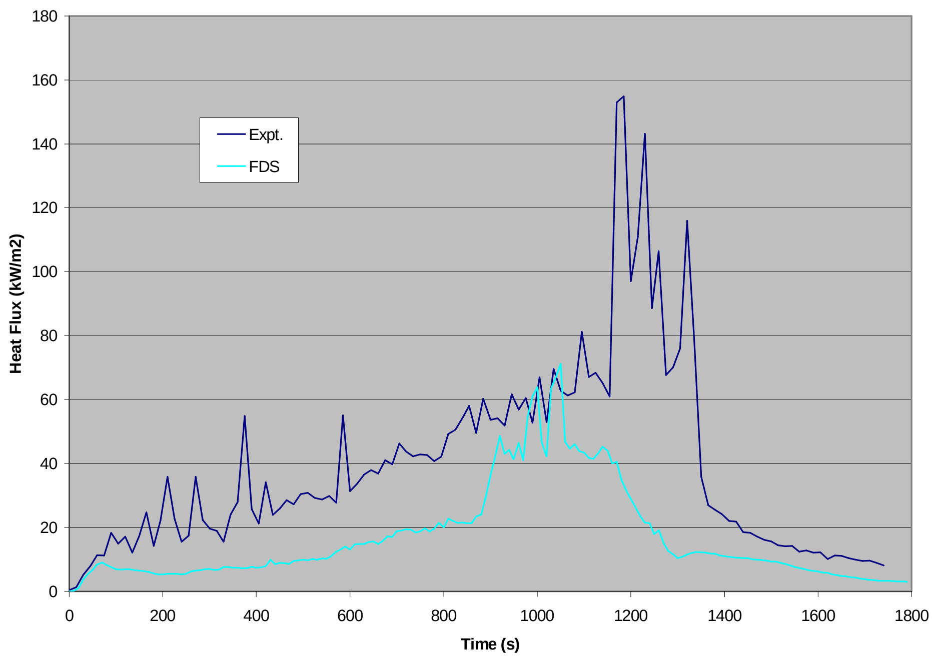

Figure 32 Heat Flux on Aerated Concrete Block (WS4) - Test 3

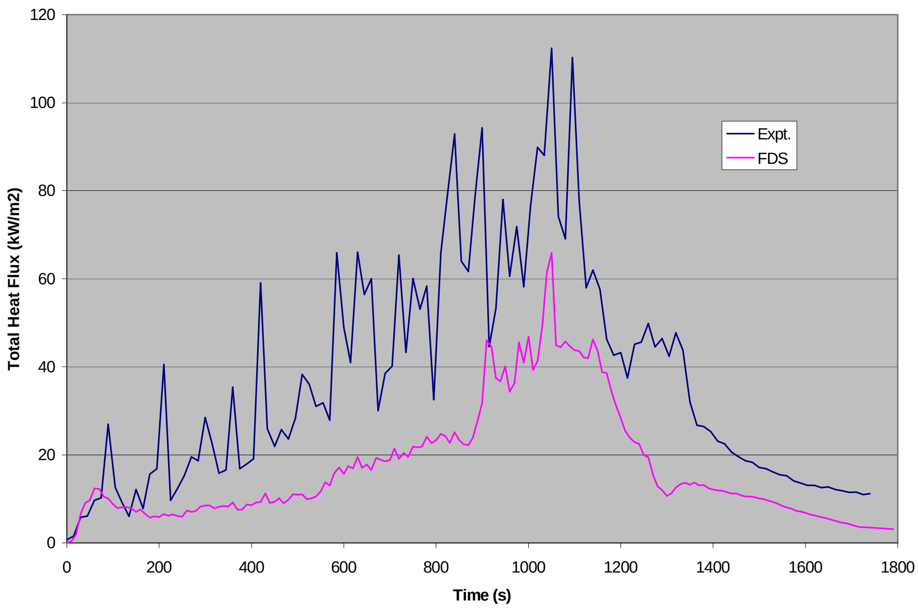

Figure 33 Heat Flux on Concrete Block (WS3) - Test 3

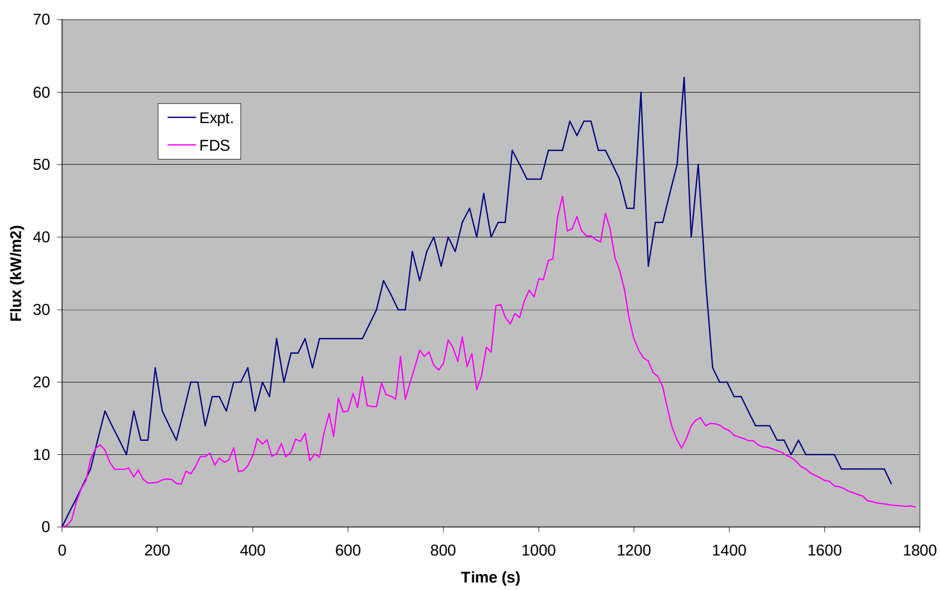

Figure 34 Heat Flux on Steel Plate (WS2) - Test 3

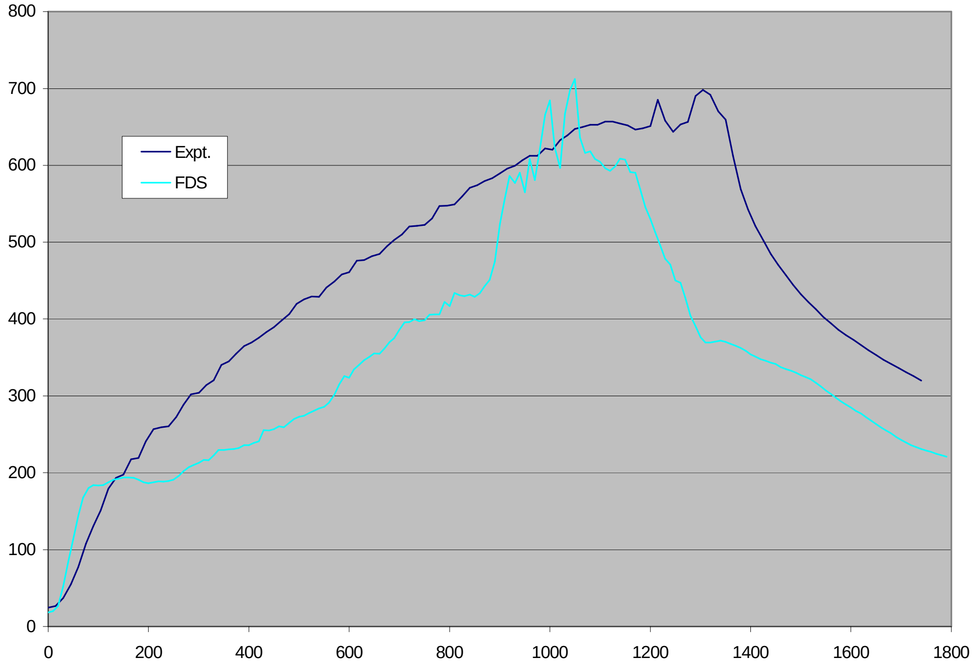

Figure 35 Aerated Concrete Block Temperature - Test 3

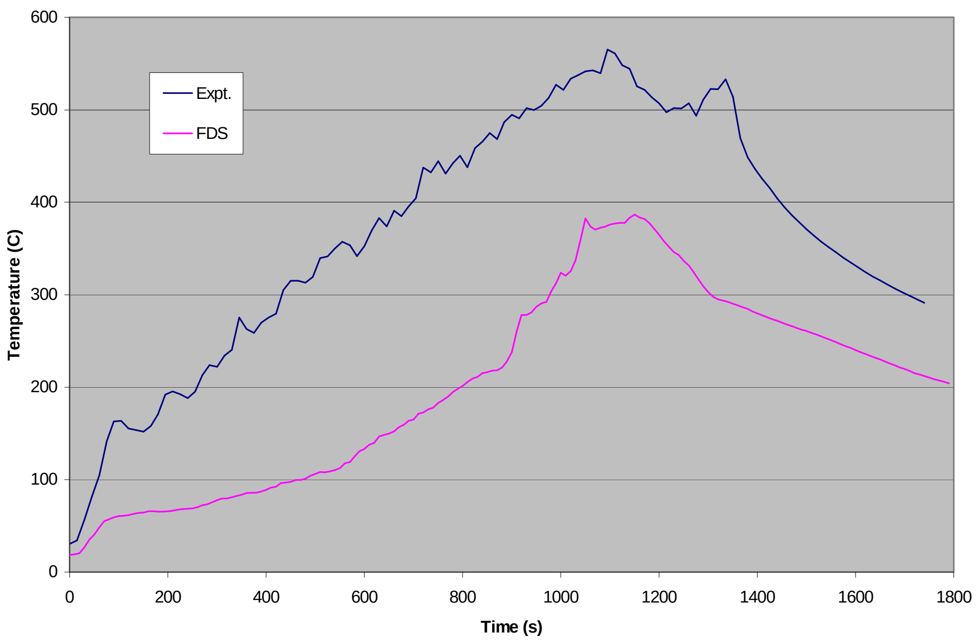

Figure 36 Concrete Block Temperature - Test 3

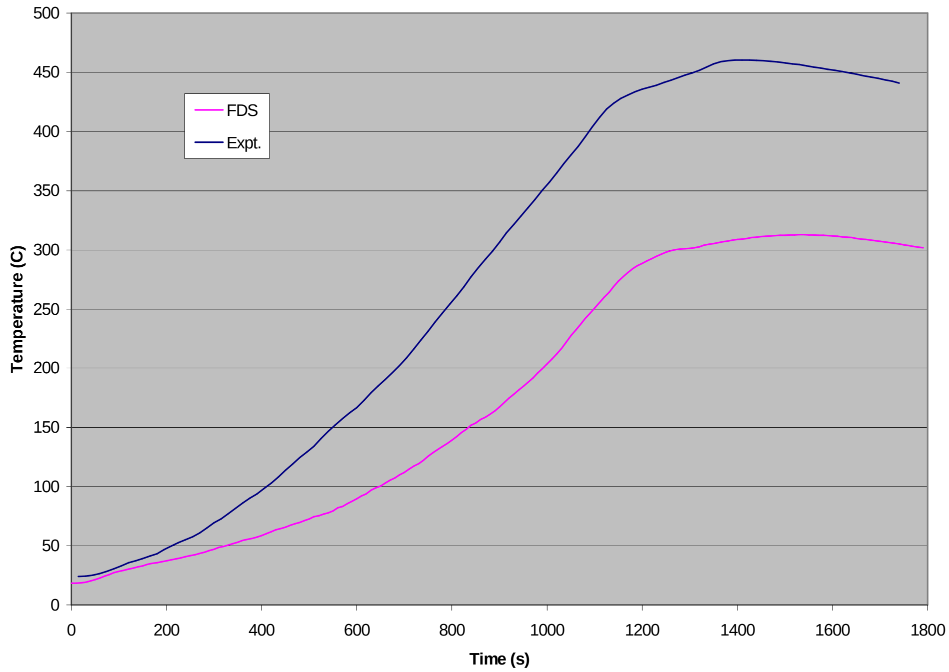

Figure 37 Steel Plate Front Surface Temperature (M34) - Test 3

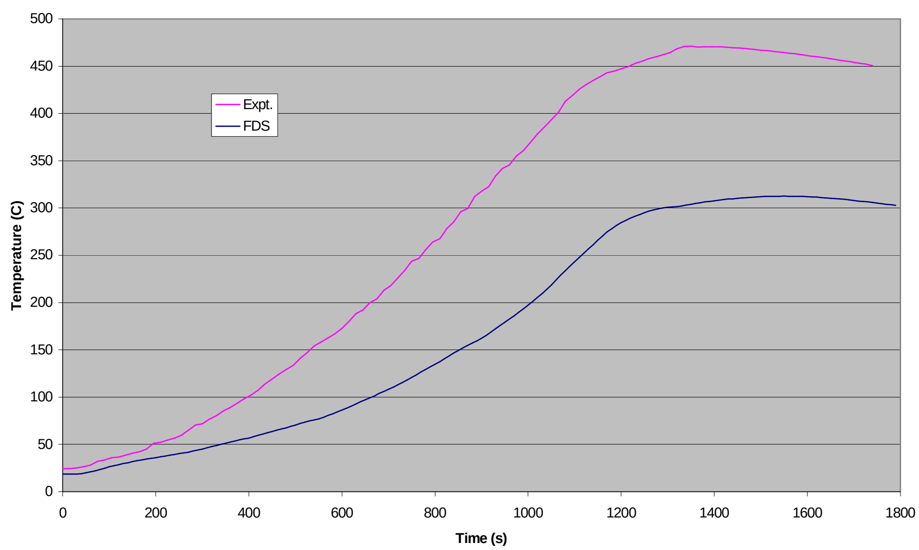

Figure 38 Steel Plate Back Surface Temperature (M35) - Test 3

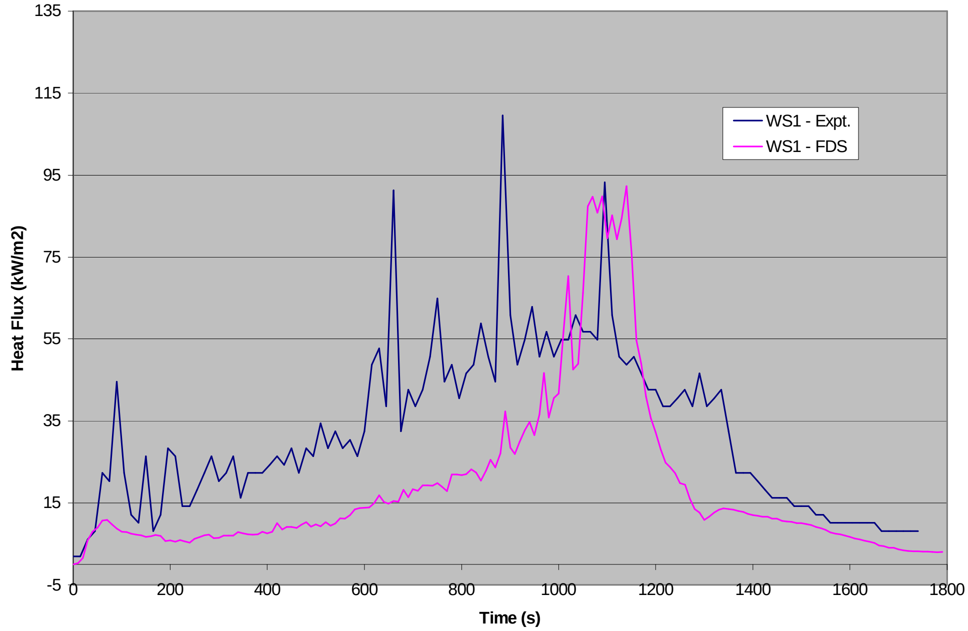

Figure 39 Heat Flux on Wall (WS1) - Test 3

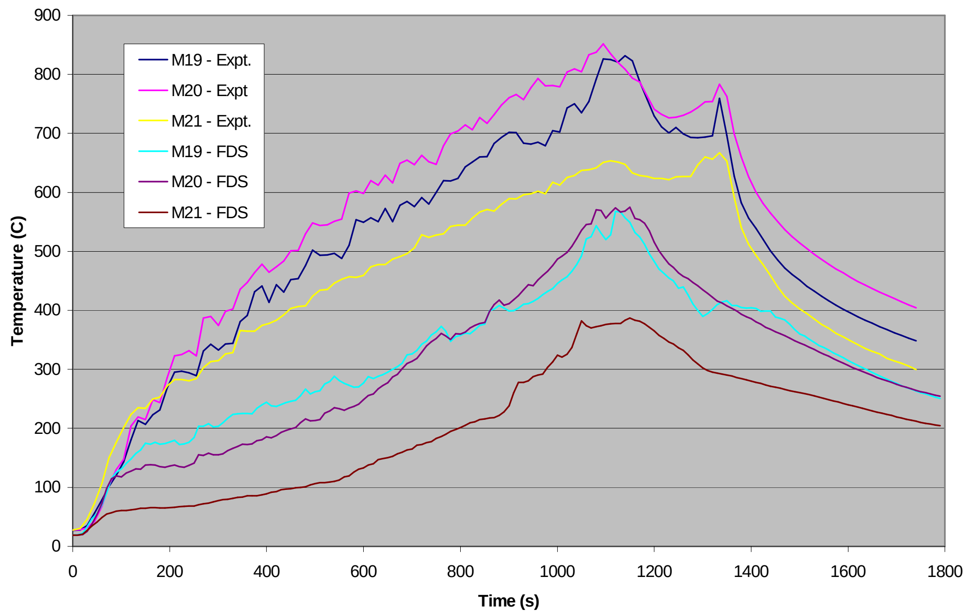

Figure 40 Wall Temperature - Test 3

Appendix A Specification of Benchmark Exercise # 4

(Prepared by GRS)

© Deytec, Inc. 2009. All rights reserved.

This document is copyrighted. It is the property of Deytec, Inc. It may be cited but not reproduced, distributed, published, or used by any other individual or organization for any other purpose whatsoever unless written permission is obtained from Deytec, Inc.

Deytec, Inc.

Nuclear Engineering Services